

## NEUROSCIENCE

# Synaptic ensembles between raphe and D<sub>1</sub>R-containing accumbens shell neurons underlie postisolation sociability in males

Ja Eun Choi<sup>1†</sup>, Dong Il Choi<sup>1†</sup>, Jisu Lee<sup>1</sup>, Jooyoung Kim<sup>1</sup>, Min Jung Kim<sup>1</sup>, Ilgang Hong<sup>1</sup>, Hyunsu Jung<sup>1</sup>, Yongmin Sung<sup>1</sup>, Ji-il Kim<sup>1</sup>, TaeHyun Kim<sup>1</sup>, Nam-Kyung Yu<sup>1</sup>, Seung-Hee Lee<sup>2</sup>, Han Kyoung Choe<sup>3</sup>, Ja Wook Koo<sup>4</sup>, Joung-Hun Kim<sup>5</sup>, Bong-Kiun Kaang<sup>1\*</sup>

Social animals expend considerable energy to maintain social bonds throughout their life. Male and female mice show sexually dimorphic behaviors, yet the underlying neural mechanisms of sociability and their dysregulation during social disconnection remain unknown. Dopaminergic neurons in dorsal raphe nucleus (DRN<sup>TH</sup>) is known to contribute to a loneliness-like state and modulate sociability. We identified that activated subpopulations in DRN<sup>TH</sup> and nucleus accumbens shell (NAc<sup>sh</sup>) during 24 hours of social isolation underlie the increase in isolation-induced sociability in male but not in female mice. This effect was reversed by chemogenetically and optogenetically inhibiting the DRN<sup>TH</sup>-NAc<sup>sh</sup> circuit. Moreover, synaptic connectivity among the activated neuronal ensembles in this circuit was increased, primarily in D<sub>1</sub> receptor-expressing neurons in NAc<sup>sh</sup>. The increase in synaptic density functionally correlated with elevated dopamine release into NAc<sup>sh</sup>. Overall, specific synaptic ensembles in DRN<sup>TH</sup>-NAc<sup>sh</sup> mediate sex differences in isolation-induced sociability, indicating that sex-dependent circuit dynamics underlie the expression of sexually dimorphic behaviors.

## INTRODUCTION

Social species make great efforts to maintain their social connections and show strong motivation of need to belong (1, 2). Social isolation disconnects the social bond and may be a form of torture in humans (3). Chronic isolation is aversive for virtually all social species and is linked to antisocial behaviors, such as depression, anxiety, and aggression (4, 5). Even an acute period of isolation influences how behaviors are expressed. Affiliative social behaviors follow periods of acute social isolation in rodents to humans (6, 7). The effects of social isolation vary by gender (8, 9). Sexual dimorphisms exist not only in brain anatomy (10) and neurological disorders (11, 12) but also in behaviors like sociability (13–17). However, sex differences in the precise neural adaptations at the synaptic and circuit levels that follow acute social isolation remain poorly understood.

The dorsal raphe nucleus (DRN) is a brain region in the central dopamine system, containing a dopaminergic population outside the ventral tegmental area (VTA) and substantia nigra pars compacta (18–20). While VTA dopaminergic neurons show strong responses in positive and negative reinforcement (21–23) and in motivated behaviors (24, 25), the DRN dopaminergic neurons (DRN<sup>TH</sup>) can promote aversion, as well as social interactions (6). Recent studies further revealed additional functions of DRN<sup>TH</sup> neurons in memory formation and arousal (26–28). However, the mechanism in neuronal circuit levels of how the DRN<sup>TH</sup> exerts its behavioral effects, or

whether it shows sexual dimorphic characteristics, remains unknown. One downstream candidate that is regulated by the dopamine system is the nucleus accumbens (NAc), which is anatomically divided into the NAc core and the NAc shell (NAc<sup>sh</sup>) (29). It is composed of two major cell types that expresses a specific family of dopamine receptors: D<sub>1</sub> receptor (D<sub>1</sub>R)-expressing and dopamine D<sub>2</sub> receptor (D<sub>2</sub>R)-expressing neurons (30). These two neuronal populations have distinct projections throughout the brain (31) and are associated with motivated behaviors, including sociability (25, 32, 33).

Because innate behaviorally activated neuronal ensembles show different intrinsic and functional properties (34), an immediate-early gene (IEG)-based tagging strategy can target these specific neuronal populations and define how the ensembles participate in behavioral responses. While the studies on specific activated populations with fear experience greatly advanced the understanding of learning and memory (35–37), many questions remain for their role with other behaviors. Recently, neuroscience has progressed to integrate activated neuronal ensembles in response to stimuli other than memory. Cocaine activates specific subpopulations of neurons in several brain regions (38–40), and these cocaine-activated neurons show enhanced connectivity in between (40), providing evidence to experience-dependent plasticity.

Now, we combined isolation experience with activity-based tagging strategy in the dopamine system. We hypothesized that such activated neuronal ensembles in DRN<sup>TH</sup>-NAc<sup>sh</sup> circuit regulate the behavioral and neurobiological responses to 24-hour social isolation in a sex-specific manner. Using optogenetics and chemogenetics combined with an IEG-based tagging system, we found that specific subpopulations of DRN<sup>TH</sup> and NAc<sup>sh</sup> neurons active during social isolation are responsible for promoting isolation-induced sociability in males but not in females. The behavioral change was accompanied by an increase in dopamine release into NAc<sup>sh</sup>. We further narrowed down this functional observation to the synaptic level and visualized the specific synapses between the isolation-activated neurons in

Copyright © 2022 The Authors, some rights reserved; exclusive licensee American Association for the Advancement of Science. No claim to original U.S. Government Works. Distributed under a Creative Commons Attribution NonCommercial License 4.0 (CC BY-NC).

<sup>1</sup>School of Biological Sciences, Seoul National University, 1 Gwanak-ro, Gwanak-gu, Seoul 08826, South Korea. <sup>2</sup>Department of Biological Sciences, Korea Advanced Institute of Science and Technology, 291 Daehak-ro, Yuseong-gu, Daejeon 305-701, South Korea. <sup>3</sup>Department of Brain and Cognitive Sciences, Daegu Gyeongbuk Institute of Science and Technology (DGIST), 333 Technojoongang-daero, Dalseong-gun, Daegu 42988, South Korea. <sup>4</sup>Emotion, Cognition & Behavior Research Group, Korea Brain Research Institute, 61, Cheomdan-ro, Dong-gu, Daegu 41062, South Korea. <sup>5</sup>Department of Life Sciences, Pohang University of Science and Technology (POSTECH), 77, Cheongam-ro, Nam-Gu, Pohang 37673, South Korea.

\*Corresponding author. Email: kaang@snu.ac.kr

†These authors contributed equally to this work.

DRN<sup>TH</sup>-NAc<sup>sh</sup>, which showed higher synaptic density only in isolated males. This synaptic strengthening occurred primarily at D<sub>1</sub>R-expressing neurons in the NAc<sup>sh</sup>. Overall, our investigations reveal sex-dependent circuit dynamics that underlie the expression of social isolation-induced sociability.

## RESULTS

### Acute social isolation alters sociability and DRN<sup>TH</sup> neuronal excitability in a sex-specific manner

To examine whether 24 hours of social isolation affects sociability differently in male and female mice, we performed the social approach task in a three-chamber arena (Fig. 1A). Socially isolated male mice showed a significant increase in sociability compared to group-housed males (Fig. 1B), but anxiety-related behavior in the open field test was not altered (fig. S1A). In contrast, female mice showed no significant difference in sociability after 24 hours of social isolation relative to group-housed females (Fig. 1C). Rather, female mice had an increase in anxiety level (fig. S1B). Because the three-chamber test might not be sensitive enough to detect the social interactions in the female mice, we further measured the level of sociability using the juvenile interaction test, in which the test mouse directly interacts with the stranger mouse (fig. S1C). Once more, increase in social interaction following 24-hour isolation was not observed in females while it was observed in males (fig. S1, D and E), consistent with the result of the three-chamber test (Fig. 1, B and C). Given that estrogen/progesterone may modulate dopaminergic function differently in brain regions (41, 42), we also tested with the ovariectomized females to determine whether female sex hormones influenced their response to isolation. However, time spent with the social target did not differ between isolated ovariectomized females and isolated sham-control females (fig. S1F). Thus, altered social interaction following

24 hours of isolation was displayed to be a sexual dimorphic phenotype, independent of sex hormones.

Neuronal excitability sets the threshold for action potential generation and regulates synaptic transmission (43). To demonstrate whether social isolation modulates neuronal excitability, we focused on DRN<sup>TH</sup> neurons, as their glutamatergic inputs and *in vivo* activity are sensitive to acute isolation (6). Using *ex vivo* whole-cell patch-clamp electrophysiology to record from DRN<sup>TH</sup> neurons, while delivering current steps, we observed a robust increase in the excitability in males following just 2 hours of isolation (Fig. 1D). However, this increase in the excitability was not observed both in nondopaminergic DRN neurons and in female mice (Fig. 1E and fig. S1G). These results suggest a mechanism that sex-dependent increased activity of DRN<sup>TH</sup> during the early phase of social isolation may trigger circuit level changes, thereby expressing the sexual dimorphic social behavior.

### Isolation-induced sociability requires DRN<sup>TH</sup> activity during isolation

We next sought to determine whether this endogenous increase in activity of DRN<sup>TH</sup> neurons during 24-hour isolation was required for the expression in social behavior following isolation. So, we used tyrosine hydroxylase (*TH*)::*cre* mice and expressed the Gi-coupled DREADD (designer receptor exclusively activated by designer drugs) hM4Di in DRN<sup>TH</sup> neurons to chemogenetically inhibit the neurons at the onset of the group-housed or socially isolated period (Fig. 1F and fig. S2C). Because we found a robust increase in excitability after 2 hours of social isolation (Fig. 1D), we delivered clozapine *N*-oxide (CNO) at the onset of isolation during this time period (44, 45). When we inhibited DRN<sup>TH</sup> neurons during isolation, the isolated mice performed as if they have not been under isolation. They spent less time with the social target compared with mice that only received saline (Fig. 1G) and showed no differences in locomotion

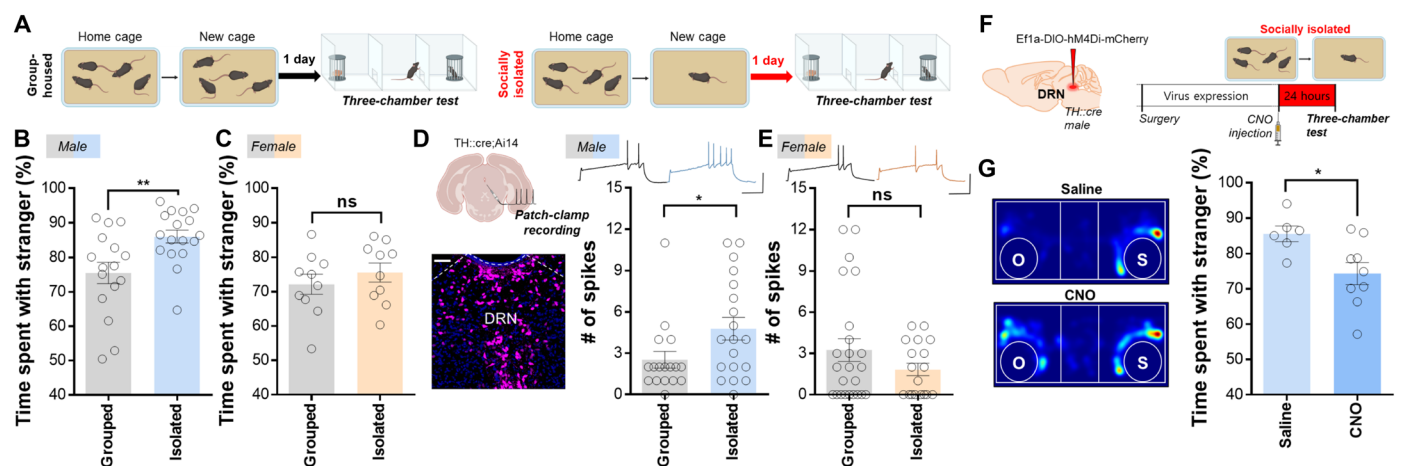


**Fig. 1. Behavioral and electrophysiological changes in DRN<sup>TH</sup> neurons following 24 hours of social isolation.** (A) Experimental scheme of group-housing and social isolation for the three-chamber test. (B) In male mice, a significant increase in time spent with the social target is detected in the socially isolated mice compared to the group-housed mice (Grouped,  $n = 16$ ,  $75.52 \pm 3.095$ ; Isolated,  $n = 17$ ,  $86.01 \pm 1.878\%$ ;  $**P = 0.0062$ ). (C) In female mice, social isolation does not alter time spent with the social target (Grouped,  $n = 10$ ,  $72.16 \pm 2.927$ ; Isolated,  $n = 10$ ,  $75.56 \pm 2.776$ ;  $P = 0.4106$ ). ns, not significant. (D) Dopaminergic neurons in DRN of *TH:cre;Ai14* mouse. Scale bar, 50  $\mu$ m. In male mice, DRN<sup>TH</sup> neuronal excitability (delivery of a 200-pA current pulse) shows a robust increase after 2 hours of isolation (Grouped,  $n = 17$  from five mice,  $2.529 \pm 0.6131$ ; Isolated,  $n = 19$ , from four mice,  $4.789 \pm 0.8257$ ;  $*P = 0.0383$ ). Example trace of grouped (black color) and isolated (blue color). Scale bar, 50 mV, 100 ms. (E) In female mice, DRN<sup>TH</sup> neurons exhibit no difference in excitability between group-housing and social isolation (Grouped,  $n = 24$  from three mice,  $3.250 \pm 0.8281$ ; Isolated,  $n = 18$  from two mice,  $1.833 \pm 0.4591$ ;  $P = 0.1798$ ). Example trace of grouped (black color) and isolated (red color). Scale bar, 50 mV, 100 ms. (F) Experimental scheme for viral injection into the DRN of *TH:cre* mice and timeline of the behavioral task. (G) Chemogenetic inhibition of the DRN<sup>TH</sup> neurons during social isolation decreases the time spent with the social target following isolation (Saline,  $n = 6$ ,  $85.51 \pm 2.237$ ; CNO,  $n = 9$ ,  $74.35 \pm 3.157$ ;  $*P = 0.0224$ ). All unpaired *t* test.

or anxiety-related behavior (fig. S2, A and B). In contrast, inhibiting DRN<sup>TH</sup> neurons during group-housing did not affect social interaction nor locomotion (fig. S2, D and E), implying that the necessity for DRN<sup>TH</sup> activity is specific to social isolation. Then, we tried to mimic the isolation-induced sharp increase in DRN<sup>TH</sup> activity by expressing hM3Dq-mCherry in group-housed males and examined whether it may artificially increase the social interactions (fig. S2, F and I). However, simply activating the DRN<sup>TH</sup> neurons did not induce any changes in the sociability and mobility levels (fig. S2, G and H). Saline-injected and CNO-injected mice without DREADD expression showed no changes in social interaction, ruling out the effect of CNO injection itself (fig. S2, J and K). Together, these results indicate that the expression of increased social behavior requires a concomitant increase in the endogenous activity of DRN<sup>TH</sup> neurons during the 24-hour isolation period.

### Isolation-activated DRN<sup>TH</sup> neuronal ensembles drive increased sociability after social isolation

We next questioned whether the subpopulation of DRN<sup>TH</sup> ensembles that are active during isolation underlie the isolation-induced sociability. To address this, we combined IEG-based tagging systems with chemogenetics to specifically label and manipulate the activated population. We used a reverse tetracycline-controlled transactivator (rtTA) driven by the *c-fos* promoter to express various proteins in a doxycycline-dependent manner (46–49). First, we examined the neuronal excitability between isolation-activated and isolation-nonactivated DRN<sup>TH</sup> neurons. We selectively captured the activated population through adeno-associated virus (AAV)<sub>2/1</sub>-Fos-rtTA and AAV<sub>2/1</sub>-TRE3G-DIO-mEmeraldNuc (nucleus-targeted mEmerald) injection into DRN of *TH::cre* mice crossed with an *Ai14* reporter mice and delivered doxycycline at the onset of the isolation period (Fig. 2, A and B). Protein expression driven by tetracycline-responsive element third generation (TRE3G) promoter was not detectable without AAV<sub>2/1</sub>-Fos-rtTA, showing the specificity of the tagging system (fig. S3, A and B). In male mice, isolation-activated DRN<sup>TH</sup> (mEmeraldNuc<sup>+</sup>/TH<sup>+</sup>) neurons showed higher excitability compared to isolation-nonactivated DRN<sup>TH</sup> (mEmeraldNuc<sup>-</sup>/TH<sup>+</sup>) neurons (Fig. 2C, left). Although isolation has been observed to induce a *c-fos* expression in female mice, we did not detect any changes in excitability between activated and nonactivated DRN<sup>TH</sup> neurons (Fig. 2C, right). These results suggest that the intrinsic properties of isolation-activated DRN<sup>TH</sup> ensembles demonstrate sexual dimorphism.

Next, we examined whether activity in the isolation-activated DRN<sup>TH</sup> neurons was required for sociability in isolated male mice. We injected AAV<sub>2/1</sub>-Fos-rtTA and AAV<sub>2/1</sub>-TRE3G-DIO-hM4Di-mCherry into the DRN of *TH::cre* mice to express hM4Di selectively in isolation-activated DRN<sup>TH</sup> neurons (Fig. 2D). We verified that the activity of these labeled neurons could be successfully suppressed by application of CNO using ex vivo whole-cell patch-clamp recording (fig. S3, C and D). Following 24 hours of isolation, we found that CNO-injected mice showed reduced sociability relative to saline-injected controls (Fig. 2E). However, CNO injection did not alter velocity nor total distance traveled (fig. S3F). These results indicate that the activated DRN<sup>TH</sup> cells during isolation experience were necessary for the expression of increased sociability. Then, we wondered whether inhibiting the group-housed-activated DRN<sup>TH</sup> neurons would affect the level of sociability. The social interaction remained intact (Fig. 2, F and G) with no changes in locomotion (fig. S3I), suggesting that the dopaminergic population in the DRN has no role in sociability

when group-housed (6). The number of activated DRN<sup>TH</sup> neurons labeled with hM4Di-mCherry were significantly higher in isolated mice than in group-housed mice (fig. S3E). To further confirm the functional specificity of isolation-activated DRN<sup>TH</sup> neurons, we performed auditory fear conditioning as DRN<sup>TH</sup> neurons were implicated in fear memory (28). We observed that fear memory fully formed although isolation-activated DRN<sup>TH</sup> neurons were inhibited (fig. S3, G and H). Together, these results suggest that the expression of isolation-induced social behavior depends on activation of this unique subpopulation of DRN<sup>TH</sup>.

To assess whether isolation-activated DRN<sup>TH</sup> population would be repeatedly activated when introduced to additional social isolation event, we conducted the isolation event two times with 1 week in between (Iso-Iso) or isolation event after group housing (Gro-Iso). Following viral expression, mice were group-housed or socially isolated for 24 hours (the first event), returned to the home cage for a week, and then exposed to social isolation (the second event) for 2 hours before perfusion (Fig. 2H). In this way, neurons active during the initial 24-hour grouped or isolated period would be labeled with mCherry, and neurons active (*fos* positive) during the final 2-hour social isolation would be immunolabeled with Alexa Fluor 488<sup>+</sup> (Fig. 2I). The proportion of [Alexa Fluor 488<sup>+</sup> mCherry<sup>+</sup>]/[mCherry<sup>+</sup>] cells (reactivation ratio) was significantly higher in the mice exposed to social isolation twice (Iso-Iso) than in the mice exposed to social isolation after group-housing (Gro-Iso; Fig. 2J), indicating that isolation-activated DRN<sup>TH</sup> neurons are not randomly activated.

### DRN<sup>TH</sup> neurons project to the NAc<sup>sh</sup>

On the basis of our findings, we next explored which downstream neural circuit drove the isolation-induced sociability mediated by DRN<sup>TH</sup> neurons. We labeled DRN<sup>TH</sup> neurons by injecting AAV<sub>1</sub>-Efla-DIO-enhanced yellow fluorescent protein (eYFP) into the DRN of *TH::cre* mice to visualize their downstream projections. Along with the innervations to central amygdala and bed nucleus of stria terminalis, we observed an axonal projection to the NAc<sup>sh</sup> (Fig. 3A) (18, 26). To further confirm the spatial accuracy of the viral spread in DRN, we injected AAV<sub>1</sub>-Efla-DIO-eYFP into DRN and AAV<sub>2/1</sub>-Efla-DIO-hM4Di-mCherry into VTA of *TH::cre* mice. DRN<sup>TH</sup> cell bodies expressed eYFP while no eYFP-expressing cell bodies were observed in the VTA, indicating that our DRN targeting parameters did not spread and label the dopaminergic neurons in the VTA (fig. S4A). Then, we bilaterally injected CAV-cre into the NAc<sup>sh</sup> of *Ai14* reporter mice to label upstream neurons and stained each DRN slice with TH to distinguish dopaminergic neurons from nondopaminergic neurons. This revealed that neurons projecting from the DRN to NAc<sup>sh</sup> are ~42% dopaminergic (Fig. 3B).

The functional connectivity between DRN<sup>TH</sup> and NAc<sup>sh</sup> was further examined through optogenetics and in vivo fiber photometry. Photoactivation of channelrhodopsin 2 (ChR2)-expressing DRN<sup>TH</sup> axons in NAc<sup>sh</sup> slices evoked an excitatory postsynaptic current in 36 of 39 neurons, with an average response of 50 pA and 4.8-ms latency (fig. S4, B and C). As previously reported, dopaminergic neurons in DRN are labeled in a high proportion through *TH::cre* mice (6), and we also verified this result by immunostaining dopamine transporter (DAT) in DRN of *TH::cre;Ai14* mice (fig. S4D). Using fiber photometry with G protein-coupled receptor activation-based dopamine (GRAB<sub>DA</sub>) sensors, we examined dopamine transmissions in the DRN<sup>TH</sup>-NAc<sup>sh</sup> circuit. AAV<sub>2/1</sub>-Efla-DIO-Chronos-mCherry was injected into DRN of *TH::cre* mice and AAV<sub>2/1</sub>-human synapsin

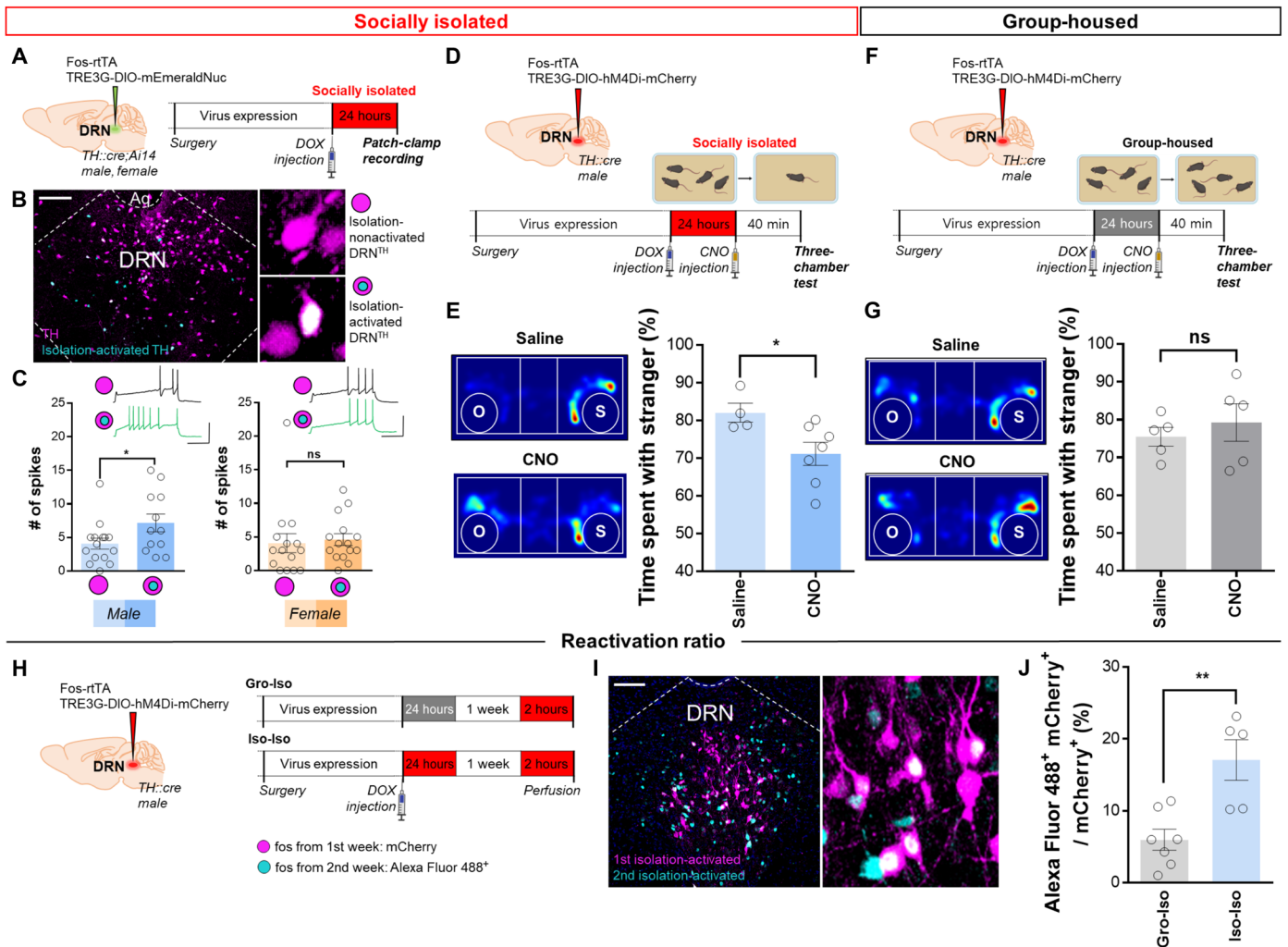


**Fig. 2. Isolation-activated DRN<sup>TH</sup> neurons are required for increased sociability after 24 hours of isolation.** (A) Experimental scheme for ex vivo patch-clamp recording. DOX, doxycycline. (B) Confocal images showing TH-positive neurons in the DRN expressing tdTomato (magenta color) and isolation-activated DRN<sup>TH</sup> neurons expressing mEmeraldNuc (cyan color). Scale bar, 100 μm. (C) Isolation-activated DRN<sup>TH</sup> (mEmerald<sup>+</sup>) neurons show a higher number of spikes (on delivery of a 200-pA current pulse) compared to isolation-nonactivated DRN<sup>TH</sup> (mEmerald<sup>-</sup>) neurons in a male-specific manner (left; mEmerald<sup>-</sup>, *n* = 15 from six mice, 4.067 ± 0.8134; mEmerald<sup>+</sup>, *n* = 12 from six mice, 7.167 ± 1.325; \**P* = 0.0480; right; mEmerald<sup>-</sup>, *n* = 15 from five mice, 4.067 ± 1.419; mEmerald<sup>+</sup>, *n* = 15 from five mice, 4.600 ± 0.8772; unpaired *t* test, *P* = 0.7516). Example traces of mEmerald<sup>-</sup> (black color) and mEmerald<sup>+</sup> (green color). Scale bars, 50 mV, 100 ms. (D and F) Schematic of virus injection and behavior schemes for labeling isolation-activated (D) and group-house-activated DRN<sup>TH</sup> neurons (F). (E) Inhibition of isolation-activated DRN<sup>TH</sup> neurons abolishes social interaction (Saline, *n* = 4, 82.01 ± 2.515; CNO, *n* = 7, 71.13 ± 3.071; \**P* = 0.0400). (G) Inhibiting the group-house-activated DRN<sup>TH</sup> neurons does not affect social interaction (Saline, *n* = 5, 75.48 ± 2.473; CNO, *n* = 5, 79.23 ± 4.934; *P* = 0.5160). (H) Schematic of the virus injection and behavioral paradigm for reactivation ratio. (I) Representative images of DRN in Iso-Iso mice. Activated DRN<sup>TH</sup> neurons through the first isolation experience are labeled with mCherry. The second isolation-activated neurons are immunostained with c-fos in Alexa Fluor 488<sup>+</sup>. Scale bar, 100 μm. (J) Reactivation ratio is significantly higher in Iso-Iso compared to Gro-Iso (Gro-Iso, *n* = 7, 5.969 ± 1.457; Iso-Iso, *n* = 5, 17.07 ± 2.814; \*\**P* = 0.0034). All unpaired *t* test.

(hSyn)-GRAB<sub>DA</sub> was injected into NAc<sup>sh</sup> with optic fiber implanted in each region. We observed an increase in GRAB<sub>DA</sub> fluorescence upon blue-light illumination in DRN indicating that DRN<sup>TH</sup> neurons released dopamine into the NAc<sup>sh</sup> (Fig. 3C), consistent with prior reports (50, 51). Collectively, dopaminergic neurons in DRN corelease glutamate and dopamine into the NAc<sup>sh</sup>.

### Optogenetic inhibition of DRN<sup>TH</sup> to NAc<sup>sh</sup> circuit suppresses isolation-induced sociability in male mice

We next examined whether the DRN<sup>TH</sup>-NAc<sup>sh</sup> circuit mediates the sociability after 24 hours of social isolation in both sexes. We injected

AAV<sub>1</sub>-Efla-DIO-eYFP or AAV<sub>1</sub>-Efla-DIO-eNpHR-eYFP into the DRN of *TH::cre* mice and implanted optic fibers bilaterally over the NAc<sup>sh</sup> (Fig. 3D). In male mice, inhibition of DRN<sup>TH</sup> terminals in NAc<sup>sh</sup> significantly diminished the increased sociability induced by social isolation (Fig. 3, E and F). This modulation occurred both in the three-chamber test and in the juvenile interaction test without a concomitant change in anxiety (fig. S4, E and F). To confirm whether this optogenetic manipulation was specific to social isolation, we performed the same experiments with the group-housed mice. Group-housed males did not show any changes in social interaction time when DRN<sup>TH</sup>-NAc<sup>sh</sup> were inhibited (Fig. 3G). As 24 hours of social

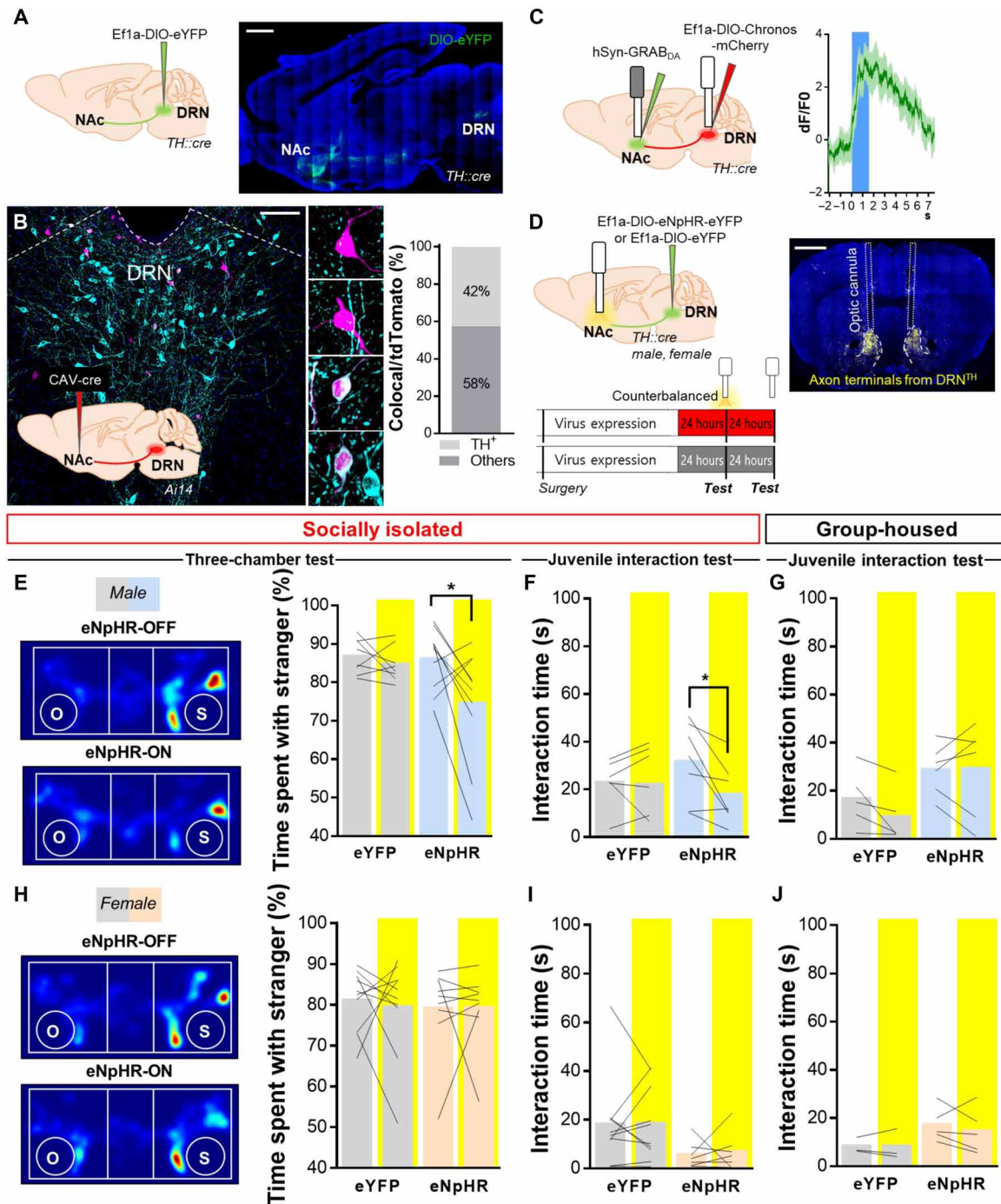


**Fig. 3. Optical inhibition of the DRN<sup>TH</sup>-NAC<sup>sh</sup> circuit suppresses social interaction following 24-hour isolation.** (A) Visualization of the axonal projections of DRN<sup>TH</sup> neurons using SeeDB2 method (scale bar, 1000  $\mu$ m). (B) Illustration of virus injection site in *Ai14* mouse. Representative image of DRN showing the monosynaptically connected tdTomato neurons (magenta) and immunostained TH-positive neurons (cyan). Scale bar, 100  $\mu$ m. Among tdTomato-labeled cells, approximately 42% were TH positive. (C) Illustration of virus-injected regions and implanted optic fibers. Changes in GRAB<sub>DA</sub> fluorescence in response to DRN<sup>TH</sup> axon terminal activation. (D) Experimental scheme for the photoinhibition of DRN<sup>TH</sup> terminals in NAC<sup>sh</sup> with group-housed and socially isolated mice. Representative image of bilateral placement of optic fiber on the eYFP-labeled axons from DRN<sup>TH</sup>. Scale bar, 1000  $\mu$ m. (E and F) In socially isolated male mice, inhibiting DRN<sup>TH</sup> to NAC<sup>sh</sup> circuit significantly suppresses social interaction time in the three-chamber test (E) (eYFP,  $n = 8$ ,  $P = 0.3424$ ; eNpHR,  $n = 10$ ,  $*P = 0.0410$ ) and in juvenile interaction test (F) (eYFP,  $n = 6$ ,  $P = 0.6937$ ; eNpHR,  $n = 7$ ,  $*P = 0.0265$ ). (G) In group-housed male mice, inhibition of DRN<sup>TH</sup>-NAC<sup>sh</sup> do not attenuate sociability (eYFP,  $n = 5$ ,  $P = 0.0803$ ; eNpHR,  $n = 6$ ,  $P = 0.9370$ ). (H and I) In socially isolated female mice, DRN<sup>TH</sup>-NAC<sup>sh</sup> circuit inhibition does not suppress the social interaction time both in the three-chamber test (H) (eYFP,  $n = 10$ ,  $P = 0.7231$ ; eNpHR,  $n = 9$ ,  $P = 0.9905$ ) and in the juvenile interaction test (I) (eYFP,  $n = 10$ ,  $P = 0.9685$ ; eNpHR,  $n = 7$ ,  $P = 0.7661$ ). (J) In group-housed female mice, inhibiting DRN<sup>TH</sup> to NAC terminals does not change the sociability level (eYFP,  $n = 3$ ,  $P = 0.9740$ ; eNpHR,  $n = 5$ ,  $P = 0.4471$ ). All paired  $t$  test.

isolation did not affect the sociability in female mice, we wondered whether manipulating the DRN<sup>TH</sup>-NAc<sup>sh</sup> circuit may affect the social interactions. Photoinhibition of the DRN<sup>TH</sup> neuronal terminals in NAc<sup>sh</sup> did not alter social behavior nor anxiety-like behavior in socially isolated and group-housed female mice (Fig. 3, H to J, and fig. S4G). Then, we refined our question to whether the sociability may be enhanced through activating DRN<sup>TH</sup>-NAc<sup>sh</sup> with AAV<sub>1</sub>-Efla-DIO-ChR2-eYFP (fig. S4H). ChR2-expressing group-housed and isolated mice in both sexes performed like eYFP-expressing control mice in the sociability level, indicating that artificially activating DRN<sup>TH</sup>-NAc<sup>sh</sup> circuit does not increase the social interactions (fig. S4, I to L). In summary, the increased sociability following 24 hours of social isolation was attenuated in males specifically by optogenetic inhibition of DRN<sup>TH</sup> to NAc<sup>sh</sup> pathway, suggesting that the DRN<sup>TH</sup>-NAc<sup>sh</sup> circuit modulates social isolation-induced sociability in a sex-dependent manner.

### Increased dopamine release in NAc<sup>sh</sup> of isolated males

We questioned whether 24 hours of social isolation actually boosts dopamine release into the NAc<sup>sh</sup>. Using GRAB<sub>DA</sub>, we recorded in vivo dopamine release in the NAc<sup>sh</sup>, while group-housed and socially isolated mice interacted with sex-matched juvenile stranger mice (Fig. 4A). We injected AAV<sub>2/1</sub>-hSyn-GRAB<sub>DA</sub> with AAV<sub>2/1</sub>-CaMKII-TagRFP-T into the NAc<sup>sh</sup> to record dopamine release and detect movement-related artifacts. In males, we observed a significantly larger increase of GRAB<sub>DA</sub> fluorescence when isolated mice undergo social interaction

compared to the signals of group-housed mice (Fig. 4, B and C). However, female mice showed no difference in the amount of dopamine release into NAc<sup>sh</sup> between isolated and group-housed (Fig. 4, D and E). Consistent with our prior data on sexual-dimorphic behavioral responses and manipulations, dopamine release in the NAc<sup>sh</sup> further provides a functional link.

### Increased synaptic density among isolation-activated DRN<sup>TH</sup>-NAc<sup>sh</sup> ensembles in isolated males

While the synaptic dynamics of glutamatergic neurons are well studied (36, 52), the synaptic dynamics of dopaminergic neurons have many open questions, especially in DRN<sup>TH</sup> neurons given the smaller dopaminergic population compared to the VTA. To examine the synaptic implications of the increased dopamine release into NAc<sup>sh</sup>, we hypothesized that social isolation may alter synaptic dynamics in the DRN<sup>TH</sup>-NAc<sup>sh</sup> circuitry to increase social interaction. Because capturing experience-activated synapses in DRN<sup>TH</sup> was difficult using traditional methods, we took advantage of our recently developed synapse labeling technique, dual-eGRASP [green fluorescent protein (GFP) reconstitution across synaptic partners] (35, 53). The dual-eGRASP technique is an advanced version of split fluorescent protein, which can emit cyan or yellow fluorescence signals when the pre- and post-eGRASP constructs are physically reconstructed in the synaptic cleft (Fig. 5A). Using dual-eGRASP, we visualized the dopaminergic synapses between DRN<sup>TH</sup> and NAc<sup>sh</sup> neurons that were activated during 24 hours of isolation.

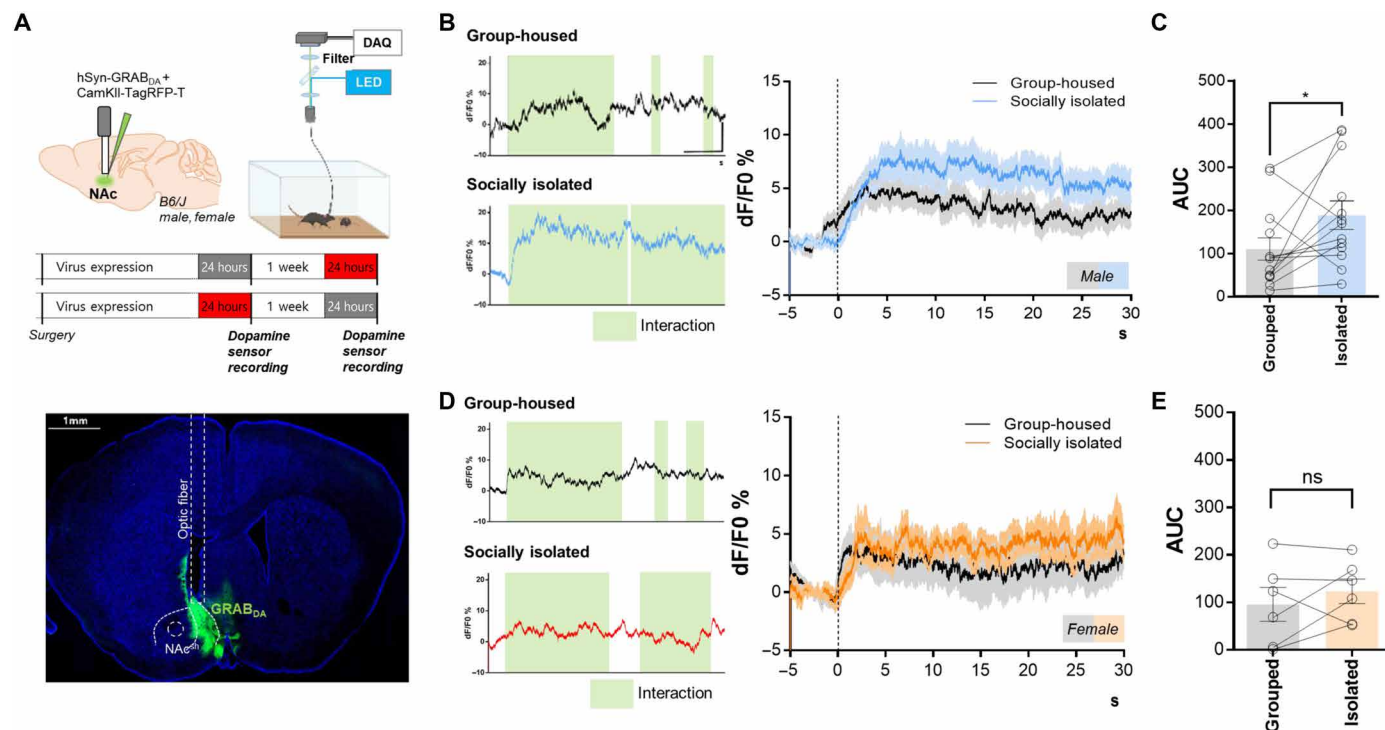


**Fig. 4. Male-specific increase of in vivo dopamine transmission in NAc<sup>sh</sup> following 24-hour isolation.** (A) Experimental schematic for in vivo fiber photometry with dopamine sensors and the expression image of GRAB<sub>DA</sub>. Scale bar, 1000  $\mu$ m. DAQ, Data acquisition; LED, Light emitting diode. (B) Representative trace of group-housed and socially isolated male mouse interacting with juvenile stranger mouse. Interaction bouts are indicated by shaded green areas. Scale bar, 10 dF/F0%, 10 s. Socially isolated mice show higher GRAB<sub>DA</sub> fluorescence compared to group-housed mice. The moment before testing when the interaction ensued was denoted as 0 s. (C) Significantly larger area under curve (AUC) in isolated mice ( $n = 13$ ; paired  $t$  test;  $*P = 0.0435$ ). (D) Representative trace of group-housed and socially isolated female mice interacting with sex-matched juvenile mouse. Interaction bouts are shown in green. Scale bars, 10 dF/F0%, 10 s. (E) Comparable AUC in group-housed and socially isolated females ( $n = 6$ ; paired  $t$  test;  $P = 0.3688$ ).

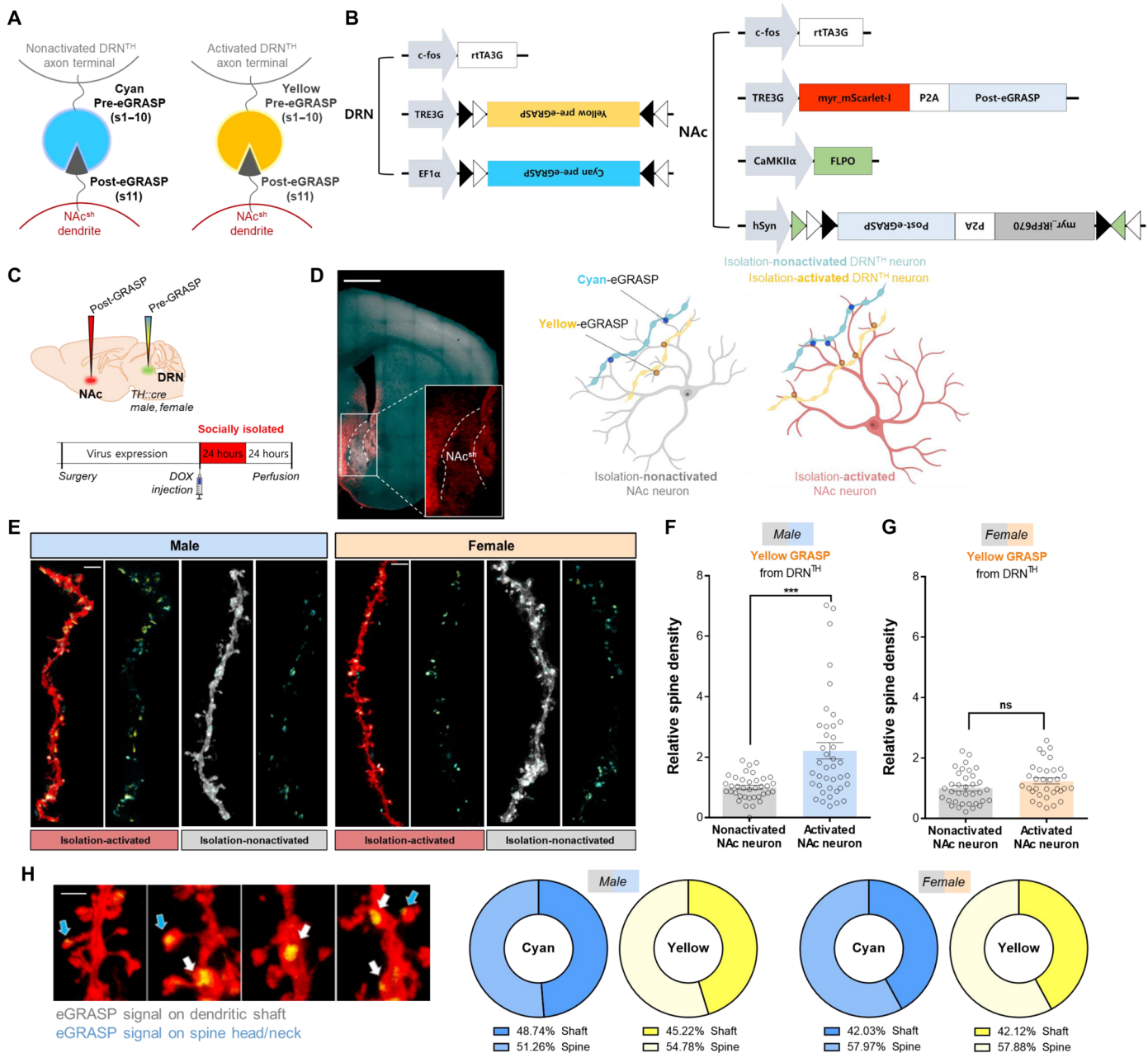


**Fig. 5. Isolated male mice show increased spine density between isolation-activated DRN<sup>TH</sup>-NAC<sup>sh</sup> neuronal ensembles.** (A) Schematics of dual-eGRASP that distinguishes the synapses depending on their inputs from DRN<sup>TH</sup> on a single NAC<sup>sh</sup> dendrite. (B) Illustration of AAV constructs and the combinations used in DRN and NAC. (C) Illustration of virus injection sites and timeline of the experimental protocol to label the synapses with dual-eGRASP. (D) Representative image of post-GRASP expressed in NAC<sup>sh</sup>. Scale bar, 1000 μm. Illustration of the four types of synapses between DRN<sup>TH</sup> and NAC<sup>sh</sup> neurons. The isolation-nonactivated NAc neurons are shown in gray, and the isolation-activated NAc neurons are shown in red. The cyan-eGRASP signals (in cyan circles) are the synapses that come from isolation-nonactivated DRN<sup>TH</sup> neurons. The yellow-eGRASP signals (in yellow circles) are the synapses that come from isolation-activated DRN<sup>TH</sup> neurons. (E) Representative images of dual-eGRASP in isolation-activated and isolation-nonactivated NAC<sup>sh</sup> dendrite with cyan-eGRASP and yellow-eGRASP puncta in both sexes. Scale bars, 5 μm. (F) In male mice, isolation-activated DRN<sup>TH</sup> neurons have higher synaptic density with isolation-activated NAC<sup>sh</sup> neurons compared to isolation-nonactivated NAC<sup>sh</sup> neurons. Each data point represents a dendrite (*n* = 37 for NAc nonactivated dendrites, *n* = 40 for NAc-activated dendrites, from six mice; Mann-Whitney two-tailed test; \*\*\**P* < 0.0001). (G) In female mice, isolation did not change spine density between the activated populations (*n* = 35 for NAc nonactivated dendrites, *n* = 33 for NAc-activated dendrites, from six mice; Mann-Whitney two-tailed test; *P* = 0.0949). (H) Representative image of dual-eGRASP signals on dendritic shaft (white arrow) and spine head/neck (blue arrow) in isolation-activated NAC<sup>sh</sup> dendrites. The percentage of cyan-eGRASP and yellow-eGRASP on dendritic shaft and spine head/neck, in isolated males and female. Scale bar, 2 μm.

To express pre-eGRASP only in DRN<sup>TH</sup> neurons in a cre-dependent manner, we designed a pre-eGRASP construct combined with a double-floxed inverted open reading frame (DIO) sequence (Fig. 5B). Yellow pre-eGRASP expression was driven by the TRE3G promoter controlled by c-fos promoter-driven rtTA3G in activated cells, and cyan pre-eGRASP was constitutively expressed by the EF1 $\alpha$  promoter. Post-eGRASP was expressed bilaterally in NAc<sup>sh</sup>, with the TRE3G promoter-driven myristoylated mScarlet-I in activated cells and myristoylated iRFP670 constitutively expressed in this neuronal population distinct from c-fos activity. Myristoylated iRFP670 was driven by the hSyn promoter with calcium/calmodulin-dependent protein kinase II (CaMKII $\alpha$ ) promoter-driven flippase (FLPO) (54). We injected the virus cocktails into the DRN and NAc<sup>sh</sup> of *TH::cre* mice and delivered doxycycline at the onset of isolation (Fig. 5C). After socially isolated for 24 hours, the mice were put back to their home cage with cagemates for an extra day to obtain a higher expression of dual-eGRASP (35, 53). Because the working time point of doxycycline is ~8 hours after injection (55), the activated synapses cannot be captured when the mice return to their home cage. We confirmed that the increased sociability following 24 hours of social isolation still remained after a further 24-hour isolation or a further 24-hour group-housing (fig. S5, A to C). Through this approach, we specifically labeled the isolation-activated DRN<sup>TH</sup> synapses as yellow-eGRASP and activity-independent synapses as cyan-eGRASP, on isolation-activated and isolation-nonactivated NAc<sup>sh</sup> neurons, respectively (Fig. 5, D and E). We validated the expression specificity under the Fos-rtTA system, such that the yellow-eGRASP and myristoylated mScarlet-I were expressed in a doxycycline-dependent manner (fig. S5D). Because iRFP670 is expressed regardless of fos expression, we analyzed nonactivated neurons that only expressed iRFP670 and without mScarlet-I expression. We performed a quantitative analysis of dual-eGRASP by reconstructing three-dimensional (3D) models using the IMARIS program (fig. S5E).

In isolated male mice, isolation-activated DRN<sup>TH</sup> neurons showed a significantly greater synaptic density with the isolation-activated NAc<sup>sh</sup> neurons compared with the nonisolation-activated NAc<sup>sh</sup> neurons (Fig. 5F). To determine whether the increased synaptic connection in males was specific to the isolation experience, we performed the same experiment with the group-housed male mice. The synaptic density did not show any differences, regardless of their activity (fig. S5F). This suggests that the higher connections between the activated ensembles were isolation specific. In isolated females, isolation-activated DRN<sup>TH</sup> neurons had a similar synaptic density with isolation-activated and nonisolation-activated NAc<sup>sh</sup> neurons (Fig. 5G). The ratio of eGRASP signals on dendritic shaft or spine head/neck did not differ between cyan-eGRASP and yellow-eGRASP in both sexes, suggesting that the activated synapses are evenly distributed on dendritic shaft and spine head/neck (Fig. 5H). Together, the male-specific increase in synaptic density extends our previous sex-dependent results and implies the sexual dimorphic involvement of activated synaptic ensembles in DRN<sup>TH</sup>-NAc<sup>sh</sup>.

### Isolation-activated neurons in the NAc<sup>sh</sup> are D<sub>1</sub>R expressing

Isolation-activated NAc<sup>sh</sup> neurons received higher synaptic connection from isolation-activated DRN<sup>TH</sup> neurons. To further elucidate the characteristics of isolation-activated neuronal population in NAc<sup>sh</sup>, we examined whether this activated population exhibits unique electrophysiological properties (Fig. 6A). Only the isolation-activated NAc<sup>sh</sup> neurons in male mice, but not in female mice, showed higher

excitability (Fig. 6B), in line with our previous observations in DRN<sup>TH</sup> (Fig. 2C). Because D<sub>1</sub>R- and D<sub>2</sub>R-expressing neurons are the two main cell types in NAc (30), we then wondered which cell types are mainly activated following isolation. AAV<sub>2/1</sub>-Fos-rtTA with AAV<sub>2/1</sub>-TRE3G-mCherryNuc was injected bilaterally into the NAc<sup>sh</sup> of D<sub>1</sub>R-eGFP and D<sub>2</sub>R-eGFP transgenic mice lines, respectively (Fig. 6C). Among the isolation-activated NAc<sup>sh</sup> neurons, we found that a significantly greater proportion of D<sub>1</sub>R-expressing neurons were labeled compared with D<sub>2</sub>R-expressing neurons (Fig. 6D).

### Inhibiting D<sub>1</sub>R-expressing neurons in the NAc<sup>sh</sup> attenuates isolation-induced sociability

To define the involvement of D<sub>1</sub>R- and D<sub>2</sub>R-expressing neurons in isolation-induced sociability, we inhibited each cell type during social interaction. First, AAV<sub>2/1</sub>-Efla-DIO-hM4Di-mCherry was bilaterally injected into the NAc<sup>sh</sup> of *D1::cre* or *D2::cre* mice to block the response to both glutamatergic and dopaminergic inputs (Fig. 6, E and G). Isolation-induced sociability disappeared when D<sub>1</sub>R-expressing neurons were inhibited during social interaction (Fig. 6F). In contrast, sociability remained intact in CNO-injected *D2::cre* mice (Fig. 6H). Inhibition of D<sub>1</sub>R- and D<sub>2</sub>R-expressing neurons did not change the mobility of the mice (fig. S6, A and B), indicating that D<sub>1</sub>R-expressing neurons are required for the expression of isolation-induced sociability. By infusing dopamine receptor antagonist intracranially into the NAc<sup>sh</sup>, we further examined whether the expression of social behavior following 24-hour isolation required the dopamine release. We bilaterally infused D<sub>1</sub>R antagonist (SCH 23390) or D<sub>2</sub>R antagonist (eticlopride) into the NAc<sup>sh</sup> 10 min before the three-chamber test (Fig. 6, I and K). The increased sociability following 24-hour isolation was abolished by D<sub>1</sub>R antagonist but not by D<sub>2</sub>R antagonist (Fig. 6, J and L). Infusions had no effect on the locomotion (fig. S6, C and D). Twenty-four hours of social isolation had no detectable effect on the protein level of D<sub>1</sub>Rs and D<sub>2</sub>Rs in NAc<sup>sh</sup> (fig. S6, E and F). These results indicate that dopamine signaling through D<sub>1</sub>Rs of NAc<sup>sh</sup> is critical for the expression of isolation-induced sociability.

## DISCUSSION

By combining IEG-based tagging methods with the dopaminergic neurons and circuits, we have identified a neuronal mechanism underlying sex-specific isolation-induced sociability. The underlying mechanism uses synaptic-level alterations in activated ensembles in DRN<sup>TH</sup>-NAc<sup>sh</sup> circuit. Dopaminergic neurons in the DRN become activated upon social interaction following 24 hours of isolation (6). We found that only male mice showed an isolation-induced enhancement in sociability, which is similar to the observed sex differences in humans (9). We speculated that neural changes during the 24-hour isolation period drove the behavioral and circuit-level changes. A subpopulation of DRN<sup>TH</sup> neurons showed a robust increase in endogenous activity during the first 2 hours of isolation. This increased activity may serve as a trigger to activate the circuit and subsequent downstream regions. When silencing DRN<sup>TH</sup> during the 24-hour isolation period, we did not detect an increase in sociability. Moreover, isolation-activated ensembles in DRN<sup>TH</sup> and NAc<sup>sh</sup> showed higher neuronal excitability, higher reactivation ratio, and higher synaptic connectivity in between. These characteristics reflect more than solely activated neurons, as activated neurons under the group-housing condition did not show these features. Together, we conclude that activated neurons during the isolation period may represent a memory

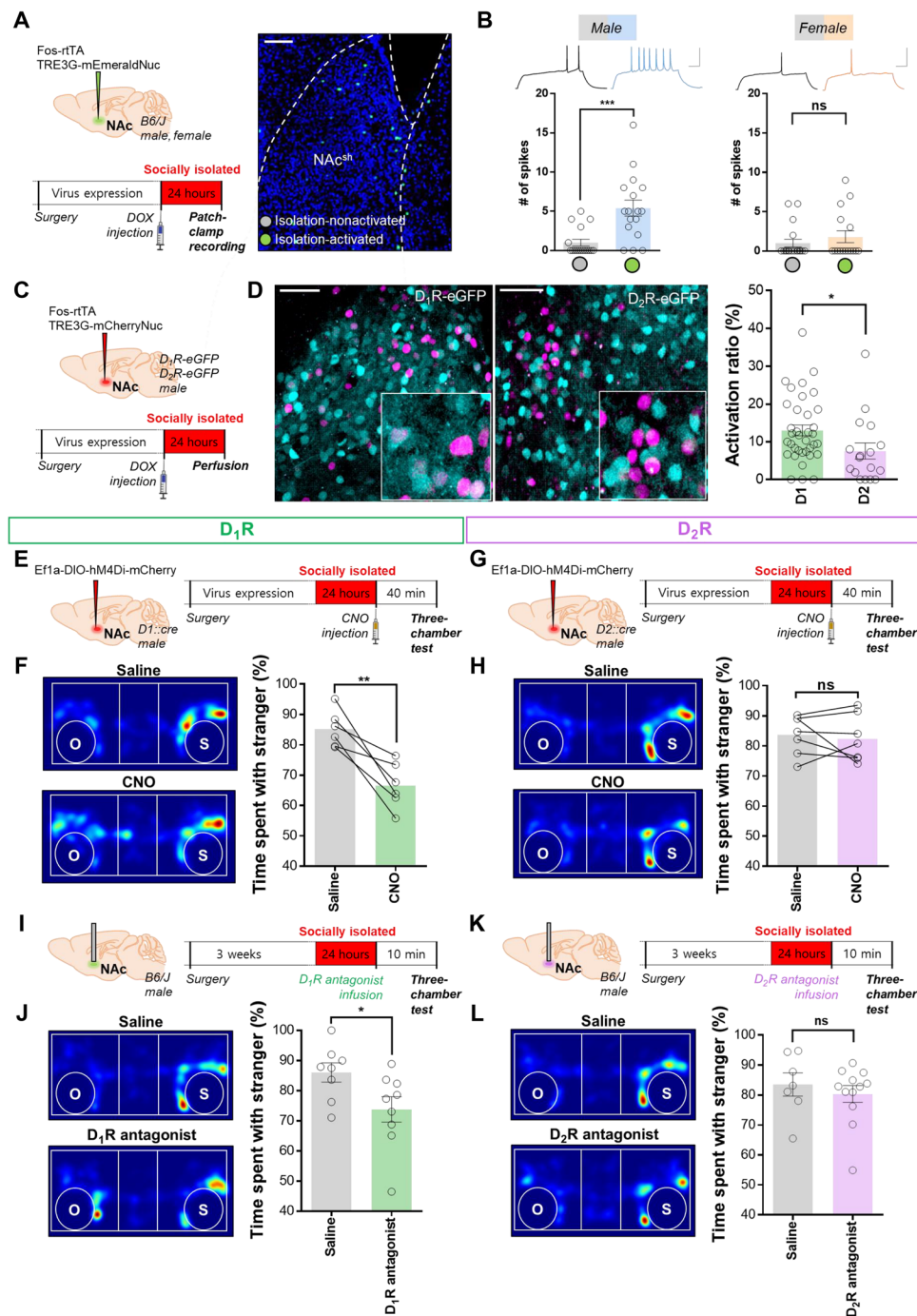


**Fig. 6. D<sub>1</sub>R-expressing neurons of NAc<sup>sh</sup> are required for sociability following isolation.** (A) Labeling of isolation-activated NAc<sup>sh</sup> neurons. Scale bar, 100 μm. (B) In isolated male mice, the neuronal excitability (delivery of a 50-pA current pulse) is significantly higher in the mEmeraldNuc<sup>+</sup> neurons (mEmeraldNuc<sup>+</sup>,  $n = 17$ ;  $1.000 \pm 0.4287$ ; mEmeraldNuc<sup>-</sup>,  $n = 17$ ;  $5.412 \pm 1.018$ ; unpaired  $t$  test; \*\*\* $P = 0.0004$ ). In isolated female mice, mEmeraldNuc<sup>+</sup> and mEmeraldNuc<sup>-</sup> neurons show comparable excitability (mEmeraldNuc<sup>+</sup>,  $n = 18$ ;  $1.000 \pm 0.4918$ ; mEmeraldNuc<sup>-</sup>,  $n = 16$ ;  $1.813 \pm 0.7595$ ; unpaired  $t$  test;  $P = 0.3656$ ). Each group from three mice. Scale bar, 50 mV, 100 ms. (C) Experimental scheme with D<sub>1</sub>R-eGFP and D<sub>2</sub>R-eGFP mice. (D) Labeling of isolation-activated NAc<sup>sh</sup> neurons. Scale bars, 50 μm. D<sub>1</sub>R-expressing neurons show higher activation ratio (mCherryNuc<sup>+</sup> eGFP<sup>+</sup>/mCherryNuc<sup>+</sup>) than D<sub>2</sub>R-expressing neurons (D<sub>1</sub>,  $n = 36$  from four mice;  $13.03 \pm 1.449$ ; D<sub>2</sub>,  $n = 17$  from two mice;  $7.543 \pm 2.126$ ; unpaired  $t$  test; \* $P = 0.0373$ ). (E and G) Experimental scheme of chemogenetically inhibiting D<sub>1</sub>R-expressing neurons (E) and D<sub>2</sub>R-expressing neurons (G) during three-chamber test. (F) Inhibition of D<sub>1</sub>R-expressing neurons abolish isolation-induced social interaction ( $n = 6$ ; paired  $t$  test; \*\* $P = 0.0054$ ). (H) Isolation-induced sociability remains intact, although D<sub>2</sub>R-expressing neurons are inhibited during the three-chamber test ( $n = 7$ ; paired  $t$  test;  $P = 0.6365$ ). (I and K) Experimental scheme of bilateral intracranial infusion of D<sub>1</sub>R antagonist (I) and D<sub>2</sub>R antagonist (K) into the NAc<sup>sh</sup> of isolated male mice. (J) Isolation-induced sociability is significantly attenuated after infusing D<sub>1</sub>R antagonist (Saline,  $n = 8$ ;  $86.03 \pm 3.214$ ; antagonist,  $n = 9$ ;  $73.79 \pm 4.218$ ; unpaired  $t$  test; \* $P = 0.0389$ ). (L) Isolation-induced sociability is not affected by D<sub>2</sub>R antagonist infusion (Saline,  $n = 7$ ;  $83.52 \pm 3.849$ ; antagonist,  $n = 12$ ;  $80.33 \pm 2.794$ ; unpaired  $t$  test;  $P = 0.5055$ ).

of social isolation experience. The male-specific increase in synaptic density between activated neuronal ensembles, coupled with a larger dopamine release into the NAc<sup>sh</sup>, provides additional mechanistic and functional insight into how circuits and synapses give rise to sexual dimorphic behaviors.

Behavioral stimuli, including social interactions, can induce changes in spine morphology (56). However, the synaptic dynamics at the afferent synapses in dopaminergic neurons, especially in activated synapses, are not well understood. Using our dual-eGRASP technique, we focused on the synaptic connections between the activated populations in DRN<sup>TH</sup>-NAc<sup>sh</sup> circuit to reveal the association between social interactions and resulting synaptic changes. Previously, a combination of dual-eGRASP with memory-encoding excitatory neurons in the hippocampus and amygdala revealed that synaptic potentiation between the activated ensembles represents memory (35, 53). Our study presented here expands this mechanism to neuro-modulatory neurons and provides insight into the synaptic changes underlying a pivotal form of social behavior. Unique features of isolation-activated DRN<sup>TH</sup> neurons include increased synapse-specific involvement with activated neuronal population, implying that isolation experiences can elicit persistent changes in DRN<sup>TH</sup> neurons. The question remains whether this visualized synaptic strengthening is presynaptically or/and postsynaptically driven. We posit that both presynaptic and postsynaptic mechanisms are involved. Isolated male mice showed higher GRAB<sub>DA</sub> signals, reflecting the increased presynaptic dopamine release. Increased dual-eGRASP spine density in isolated male mice may occur by a postsynaptic mechanism. These observations appear to be isolation specific and sexual dimorphic, such that group-housing experience and female mice did not show the differences between activated and nonactivated neurons. Our results provide an initial indication of the underlying synaptic mechanisms in sexual dimorphism. Because 2 weeks of social isolation permanently changed the sociability of males (57), our study prompts further examination of the persistent synaptic changes in DRN<sup>TH</sup>-NAc<sup>sh</sup>.

The complex functions of dopamine have not coalesced around a single function. Several studies indicate that dopaminergic neurons corelease glutamate (6, 58, 59) and heterogeneity among DRN<sup>TH</sup> exists (20, 60). Our observations further imply that the subpopulation of DRN<sup>TH</sup> neurons, which corelease dopamine/glutamate into the NAc<sup>sh</sup>, contribute to the visualized synaptic strengthening. Because dopaminergic neurons can synapse on the neck of dendritic spines and form a triadic circuit with glutamatergic (nondopaminergic) synapses (61, 62), the increased synaptic density between activated ensembles in DRN<sup>TH</sup>-NAc<sup>sh</sup> may occur by multiple scenarios: (i) The very same activated synapses receive other glutamatergic inputs or (ii) presynaptic DRN dopaminergic release acts on the axonal arbors of dopamine/glutamate coreleasing neurons itself. In either case, the synaptic strengthening appears to specifically occur in activated NAc<sup>sh</sup> neurons, as nonactivated NAc<sup>sh</sup> neurons did not show increased synaptic features. We visualized evenly distributed activated contacts on the synaptic head/neck and dendritic shaft, further suggesting that additional glutamatergic input may be less important.

Multiple inputs to the NAc, which is subdivided into central core and surrounding shell (63), regulate social behaviors by acting on integrating accumbal microcircuits modulated primarily by gamma-aminobutyric acid (GABA)ergic, glutamatergic, and dopaminergic signaling. The neuronal projections of the core remain within the basal ganglia and serve to evaluate reward-related actions. In contrast,

the shell is interconnected with regions outside the basal ganglia to drive motivation and reward-related processes (64, 65). We observed that DRN<sup>TH</sup> neurons only project to the shell of NAc. This is in contrast to VTA<sup>TH</sup> neurons, which project to both NAc shell and core (66). We suggest that the anatomical projections from DRN<sup>TH</sup> to the NAc<sup>sh</sup> drive motivated responding to increase social interactions after isolation. We posit that this circuit exclusively uses D<sub>1</sub>R-expressing neurons in NAc<sup>sh</sup>, as our inhibition experiments revealed the functional involvement of D<sub>1</sub>R, but not D<sub>2</sub>R in isolation-induced sociability although the activation of D<sub>1</sub>R-expressing neurons can affect D<sub>2</sub>R-expressing neurons (67). Our results are consistent with reports that the activity of D<sub>1</sub>R-expressing neurons in the NAc is important for modulating social behavior (25, 68).

A challenging question is how the brain can generate sexually dimorphic social behaviors. The behavioral effect of 24-hour social isolation in both sexes are markedly different, as isolated males show higher sociability levels, while isolated females show higher anxiety levels (8, 69). Modulation of DRN<sup>TH</sup>-NAc<sup>sh</sup> circuit only affected isolation-induced sociability, not isolation-induced anxiety in females, suggesting the distinct circuits to yield different sexual dimorphisms.

Impairment in social interaction is one trait of autism spectrum disorders (ASDs), as social isolation and loneliness can occur in patients with ASD (70, 71). Moreover, ASD shows a 4:1 gender distribution of males:females, although the treatment of sexual dimorphism in patients with ASD remains very broad (72, 73). Although complex interactions may exist between neural circuits that govern social behavior, increased sociability following social isolation and our proposed underlying mechanism associated with sexual dimorphic DRN<sup>TH</sup>-NAc<sup>sh</sup> circuit likely provide additional characteristics of ASD pathophysiology. We speculate that our study may inform further treatments to enhance social participation in both genders to reduce the prevalence of loneliness.

In conclusion, our findings reveal the underlying neural mechanism of sexual dimorphism in social isolation that bridges the synaptic, cellular, and circuit levels to behavior. We propose that modulating this circuit may treat gender-specific deficiencies in sociability found in ASD.

## MATERIALS AND METHODS

### Animals

All mice used in this study were maintained in a C57BL/6J background. Depending on the experiments, male or/and female mice were used with information mentioned in the figures or figure legends. Animals were housed with food and water ad libitum on a 12-hour light-dark cycle and were housed in four to six animals per cage before being group-housed or socially isolated. *TH::cre* (JAX008601) mice were crossed with *Ai14* reporter mice (JAX007914) to visualize dopamine neurons in a cre-dependent manner (74). D1-eGFP (MMRRC000297) and D2-eGFP (MMRRC000230), *D1::cre* (MMRRC036916) and *D2::cre* (MMRRC032108) mice were used to visualize and target D<sub>1</sub>R- and D<sub>2</sub>R-expressing neurons in NAc<sup>sh</sup> (75, 76). The number of animals used in each experiment is noted in the figure legends. All mice were 8 to 18 weeks old during experiments. Eight- to 12-week-old mice underwent stereotaxic surgery, and all experiments were completed within 6 weeks. All experimental procedures were approved by the Institutional Animal Care and Use Committee of Seoul National University.

### Stereotaxic surgery

Mice (8 to 12 weeks) were anesthetized with a ketamine/xylazine solution and positioned on a stereotaxic apparatus (Stoelting Co.). The virus mixture was injected into target regions through a 32-gauge needle with a Hamilton syringe at a rate of 0.1  $\mu\text{l}/\text{min}$ , and the total injection volume per site was 0.3 to 0.5  $\mu\text{l}$ . The needle tip was positioned 0.05 mm below the target coordinate right before the injection for 2 min. After the injection was completed, the needle remained in place for an additional 7 min and was withdrawn slowly. The stereotaxic coordinates for each target site were as follows: NAc (AP: +1.5; ML:  $\pm 0.65$ ; DV:  $-4.55$ ), VTA (AP:  $-2.9$ ; ML:  $\pm 0.7$ ; DV:  $-4.65$ ), and DRN (AP:  $-4.2$ ; ML: 0; DV:  $-3.2$ ). For bilateral cannula implantations, cannula (custom and Newdoon) were implanted 0.5 mm above NAc<sup>sh</sup> and held in place with dental cement.

### IEG-based tagging system

An activity-dependent tagging system was used as previously reported (53). Fos-rtTA and TRE3G promoter-based Tet-on labeling strategy was used (35, 48, 77). When rtTA proteins are expressed in fos-expressing neurons, it will bind to TRE3G promoter under doxycycline-presenting conditions. The working time point of doxycycline is  $\sim 8$  hours after injection; thus, events longer than 24 hours cannot be captured (55). Subsequently, DNA constructs downstream of TRE3G promoter are induced.

### Chemogenetic manipulations

The designer drug CNO (10 mg/kg for inhibition, 3 mg/kg for activation, i.p.; Hellobio) was administered 40 min before the behavioral tasks. CNO (5  $\mu\text{M}$ ) was used for ex vivo patch-clamp recording, and the effect was measured 10 min after CNO perfusion.

### Optogenetic manipulations

Optical activation (23) was achieved by delivering 473-nm, 20-Hz train of eight pulses of 5-ms pulse width (6). Optical inhibition delivered constant 593 nm. AAV<sub>1</sub>-Efla-DIO-eYFP served as the control for both activation and inhibition experiments. Behavior tasks were performed after 4 weeks of viral expression.

### Electrophysiology

Adult mice of both sexes were anesthetized with isoflurane, and their brains were quickly dissected. *N*-methyl-D-glucamine (NMDG) solution (93 mM NMDG, 2.5 mM KCl, 1.2 mM NaH<sub>2</sub>PO<sub>4</sub>, 30 mM NaHCO<sub>3</sub>, 20 mM Hepes, 25 mM glucose, 5 mM sodium ascorbate, 2 mM thiourea, 3 mM sodium pyruvate, 10 mM MgSO<sub>4</sub>, and 0.5 mM CaCl<sub>2</sub>) was used during brain slicing and recovery (35). Transverse slices (250  $\mu\text{m}$  for DRN and 300  $\mu\text{m}$  for NAc) were prepared in an ice-cold NMDG solution with a vibratome and then recovered in a 32°C NMDG solution for 6 to 7 min. After at least 1 hour of recovery in artificial cerebrospinal fluid (ACSF; 124 mM NaCl, 2.5 mM KCl, 1 mM NaH<sub>2</sub>PO<sub>4</sub>, 25 mM NaHCO<sub>3</sub>, 10 mM glucose, 2 mM CaCl<sub>2</sub>, and 2 mM MgSO<sub>4</sub>), the slice was placed in the recording chamber perfused with 32°C ACSF. To obtain reliable recordings, patched cells were allowed to stabilize for at least 3 min, and resting membrane potential was then recorded with no injected current. Only cells with a change in access resistance  $< 20\%$  were included in the analysis. The recording pipettes (2 to 4 megohm) were filled with an internal solution containing 145 mM K-gluconate, 5 mM NaCl, 10 mM Hepes, 1 mM MgCl<sub>2</sub>, 0.2 mM EGTA, 2 mM MgATP, and 0.1 mM Na<sub>3</sub>GTP (280 to 300 mOsm, adjusted to pH 7.2 with KOH).

For combination with optogenetics, neurons that exhibited an average current (over four sweeps) of  $\geq 10$  pA recorded at  $-70$  mV were defined as connections.

### Behavior tasks

#### Three-chamber test

During the habituation session, mice were allowed to freely move in the apparatus for 10 min. After the habituation, an unfamiliar juvenile mouse (stranger) was placed under one cup and an object was placed under the other cup (78). Then, the test mice were recorded for the preference to the sex-matched unfamiliar juvenile mouse for 10 min, which is the test session. The time of sniffing to each cup (stranger and object) was analyzed. Time spent sniffing the stranger was divided by the total time of sniffing both stranger and object, which was regarded as sociability. Ethovision software generated the heatmaps and analyzed the velocity and total distance moved.

#### Juvenile interaction test

During the first 1 min, test mice were placed in a cage with new bedding for habituation. Then, sex-matched juvenile stranger mice were introduced into the cage for 5 min. Every task used new bedding. Observers counted the interaction time, which included nose-to-nose sniffing and nose-to-anogenital sniffing.

#### Open-field test

Mice were gently placed in the center and left to explore the chamber for 10 min. After every task, the chamber was cleaned with 75% ethanol and water. The total distance moved and the time spent in the center were analyzed using the Ethovision software (79).

#### Auditory fear conditioning

Auditory fear conditioning occurred in two different contexts (context A and context B) to minimize the influence of contextual associations. Context A was a square chamber with steel grid floor (Coulbourn Instruments; H10-11 M-TC), and context B was a rectangular plastic box with striped walls and a hardwood laboratory bedding (Beta Chip). For fear conditioning, mice were placed in context A and could explore the context for 150 s, followed by three exposures to auditory tone CS (30 s), each of which coterminated with 2 s, 0.75-mA footshock US, with a 30-s intertrial interval. After conditioning, mice were immediately placed in their home cages. One day after conditioning, mice were placed into a previously unexperienced context B and exposed to the auditory tone to measure the freezing behavior. Freezing behavior was recorded and scored using a video-based FreezeFrame fear-conditioning system.

#### Brain clearing

SeeDB2 protocol (80) was used for brain clearing. The brain sample was perfused with 4°C chilled 1 $\times$  phosphate-buffered saline (PBS) and 4% paraformaldehyde (PFA) in 1 $\times$  PBS. Perfused brains were fixed in 4% PFA for 12 hours. Samples were sliced by a vibratome into 1-mm thickness for clearing. All SeeDB2 incubation procedures were performed at room temperature.

#### Sample preparation and confocal imaging for dual-eGRASP

All viruses used for dual-eGRASP were confirmed in prior reports (35, 53). AAV<sub>2/1</sub>-CamKII-FLPO and AAV<sub>2/1</sub>-hSyn-FRT (flippase recognition target site)-Floxed-myriRFP670V5-P2A-post-eGRASP were newly constructed in this paper. Perfused brains were fixed with 4% PFA in PBS overnight at 4°C and dehydrated in 30% sucrose in PBS for 2 days at 4°C. Brains were sliced into 50- $\mu\text{m}$  sections for dual-eGRASP analysis. Sections were mounted in Vectashield mounting

medium (H-1000, Vector Laboratories). For dual-eGRASP analysis, NAc dendrites were imaged in Z-stack using a Leica SP8 confocal microscope with a 63× objective and distilled water immersion.

### Image analysis for dual-eGRASP

Processing the confocal image and 3D reconstruction of dendrites were performed using IMARIS (Bitplane, Zurich, Switzerland) software. Before analysis, all image samples were blinded to exclude any bias. Each mScarlet-I–positive or iRFP670–positive dendrite was manually marked as a filament, while hiding other fluorescent signals. iRFP670–only dendrites were chosen for nonactivated ones. Each cyan- or yellow-eGRASP signal was marked as a cyan- or yellow-sphere through IMARIS automatic detection. Cyan- and yellow-eGRASP puncta on dendrites were manually counted, and overlapped cyan- and yellow-eGRASP signals were considered yellow signals.

Every confocal image had all four colors for normalization (iRFP–only–expressing and RFP–expressing dendrites, as well as cyan- and yellow-eGRASP signals). The spine density data were exported in blind to the experimenter. Then, the raw data for each dendrite were paired with the GRASP information (cyan, yellow, or no GRASP). Dendrites without any cyan-eGRASP were excluded for a more precise analysis. For normalization within one confocal image, the raw value of yellow density on every iRFP dendrite was averaged. Then, the raw value of each yellow density on iRFP dendrite and yellow density on mScarlet dendrite were divided by the calculated average. This normalized value was used for further statistical analysis.

### Immunohistochemistry

Brains were postfixed in 4% PFA at 4°C overnight and transferred to 30% sucrose for 2 days at 4°C. Brains were embedded in optimal cutting temperature mounting medium, and 40- $\mu$ m sections were cut using a cryostat (Leica). For immunohistochemistry, primary antibodies rabbit anti-TH (AB152; Millipore), chicken anti-TH (ab76442; Abcam), rat anti-DAT (MAB369, Sigma-Aldrich) and rabbit anti-c-fos (sc-52; Santa Cruz Biotechnology, 226003; SySy) were diluted to 1:300 to 1:1000 in blocking solution and incubated for 24 hours at 4°C. Secondary antibodies in the blocking solution were incubated for 2 hours at room temperature, and sections were mounted with Vectashield. Images were viewed under Zeiss LSM 700 and Leica SP8 confocal microscopes.

### Ovariectomy

Juvenile female mice (5 to 7 weeks of age) were ovariectomized under subcutaneous injections of ketamine. The fallopian tubes were traced, both ovaries were removed, and the skin was sutured. For the control group, the cagemates of ovariectomized mice were selected and subjected to sham surgery. After 3 to 4 weeks of recovery in the home cage, the ovariectomized and sham groups underwent the behavioral tasks.

### Western blot

Following 24 hours after group-housing or social isolation, the brains were rapidly removed. The NAc<sup>sh</sup> was dissected under a dissecting microscope and immediately frozen with liquid nitrogen. Samples were homogenized in radioimmunoprecipitation assay buffer containing 50 mM TrisCl at pH 7.6; 150 mM NaCl; 1 mM EDTA; 1 mM dithiothreitol; 1% NP-40; 0.1% SDS; 0.5% sodium deoxycholate. The protein concentration was quantified using a Pierce BCA protein assay kit (Thermo Fisher Scientific) following the manufacturer's protocol. Protein samples were electrophoresed on a 4 to 12% gradient gel

(Invitrogen, NW04125BOX) and transferred to a nitrocellulose blotting membrane (GE Healthcare, 10600003). The membranes were blocked with 5% skim milk and incubated with primary antibodies: D<sub>1</sub>R (1:500; AB1765P, Merck Millipore), D<sub>2</sub>R (1:500; AB5084P, Merck Millipore), and pan-cadherin (1:5000; sc-59876, Santa Cruz Biotechnology) overnight at 4°C. Blots were rinsed out three times in 1X Tris-Buffered Saline, 0.1% Tween<sup>®</sup> 20 (TBST) and exposed to secondary antibody at room temperature for 2 hours: goat anti-mouse immunoglobulin G (IgG; 1:1000; Q-11071MP, Invitrogen) or goat anti-rabbit IgG (1:1000; A0545, Sigma-Aldrich). Bands were visualized using a Chemiluminescent horseradish peroxidase substrate kit (Millipore Corporation, Billerica, MA 91821, USA) and ChemiDoc XRS+ (721BR02655, Bio-Rad). Signals were detected and quantified using ChemiDoc MP device (Bio-Rad).

### Intracranial drug delivery

Twenty-six–gauge guide cannulas were implanted bilaterally into the NAc (AP: +1.4; ML:  $\pm$ 1.5; DV: –4.0) at a 14° angle. After recovery, the mice were injected bilaterally with 0.3  $\mu$ l of either 5 mM SCH23390 (Tocris) or 1 mM eticlopride (Sigma-Aldrich) or saline vehicle in the NAc<sup>sh</sup>. The 30-gauge needle was injected 0.2 mm lower than the guide cannula. After the volumes were injected, it was left in place for 3 min to allow diffusion. Three-chamber tests were started 10 min after infusion.

### Fiber photometry

We used *TH::cre* mice to detect dopamine release from DRN<sup>TH</sup> in NAc<sup>sh</sup>. The dopamine sensor AAV<sub>2/1</sub>-hSyn-GRAB<sub>DA</sub> (Addgene 113050) was injected into the NAc<sup>sh</sup> (AP: +1.5; ML: 0.65; DV: –4.5) with optic fiber (400- $\mu$ m core diameter, AP: +1.5; ML: 0.65; DV: –4.4), and AAV<sub>2/1</sub>-Efla-DIO-Chronos-mCherry [further modified from a previous paper (35)] were injected into the DRN (AP: –4.2; ML: 0; DV: –3.2) with optic fiber (200- $\mu$ m core diameter, AP: –4.2; ML: 0; DV: –2.8). For combination with social interaction following group-housed and socially isolated mice, wild-type mice were injected with AAV<sub>2/1</sub>-hSyn-GRAB<sub>DA</sub> and AAV<sub>2/1</sub>-CamKII-TagRFP-T. Fibers were implanted in NAc<sup>sh</sup> (400- $\mu$ m core diameter, AP: +1.5; ML: 0.65; DV: –4.4). All experiments were performed at least 1.5 weeks after surgery for recovery.

For the optogenetic fiber photometry experiment, we placed the test mouse into a rectangular acrylic cage for a habituation period of least 5 min. After habituation, we recorded GRAB<sub>DA</sub> responses in NAc<sup>sh</sup>. During measurements, we delivered blue light (10 mW) into the DRN at 30-s intervals for 1.5 s to activate DRN<sup>TH</sup> neurons.

For fiber photometry combined with behavior, 24-hour group-housed or isolated mice were placed in rectangular acrylic cage and habituated over 5 min to stabilize before measuring the baseline dopamine signals in NAc<sup>sh</sup>. The secondary virus (AAV<sub>2/1</sub>-CamKII-TagRFP-T) assessed motion artifacts before the GRAB<sub>DA</sub> recordings (whether the cannula had not shifted and was well connected to the sleeve while the animal was freely moving). After this habituation period, we recorded GRAB<sub>DA</sub> signals for 60 s to measure the dopamine response at baseline. After baseline recording, we introduced sex-matched juvenile mouse into the cage and measured the dopamine signals for 60 s at the onset of social interaction. Then, we withdrew the juvenile mouse and recorded an additional 60 s of dopamine responses.

Fiber photometry analysis was performed as previously published (81). Fluorescence signals were measured by the Doric studio (ver 5.3.3.14) program. To measure the dopamine dynamics in NAc<sup>sh</sup>, the moment immediately before the test mouse interacted with a

juvenile mouse was denoted as 0 s. Next, we calculated  $(F - F_0)/F_0$  ( $\Delta F/F$ )%. We considered  $F_0$  as the baseline fluorescence signal averaged over a 3-s time window between  $-4$  and  $-1$  s before the social interaction starts. We analyzed and plotted the dopamine dynamics for the first 30 s after the social interaction started.

### Quantification and statistical analysis

All behavioral data were scored by a trained observer blind to experimental conditions or scored using an automated system (Ethovision). Then, data were processed and analyzed using Excel and GraphPad Prism 8. Statistical analyses were conducted using unpaired  $t$  tests, paired  $t$  test, two-way analysis of variance (ANOVA), and Mann-Whitney two-tailed test when appropriate. Unless specified otherwise, all data are shown as mean values  $\pm$  SEM with the  $n$  value for each dataset. Statistically significant effects are reported in the figure legend. The significance threshold was held at 0.05, two-tailed (not significant, ns,  $P > 0.05$ ; \* $P < 0.05$ ; \*\* $P < 0.01$ ; \*\*\* $P < 0.001$ ; \*\*\*\* $P < 0.0001$ ). No exclusion of any data was performed.

### SUPPLEMENTARY MATERIALS

Supplementary material for this article is available at <https://science.org/doi/10.1126/sciadv.abo7527>

[View/request a protocol for this paper from Bio-protocol.](#)

### REFERENCES AND NOTES

- R. F. Baumeister, M. R. Leary, The need to belong: Desire for interpersonal attachments as a fundamental human motivation. *Psychol. Bull.* **117**, 497–529 (1995).
- P. L. P. Van Loo, A. C. de Groot, B. F. M. Van Zutphen, V. Baumans, Do male mice prefer or avoid each other's company? influence of hierarchy, kinship, and familiarity. *J. Appl. Anim. Welf. Sci.* **4**, 91–103 (2001).
- R. H. Thoenig, Solitary confinement-punishment within the letter of the law, or psychological torture. *Wisconsin Law Rev.*, 223–311 (1972).
- J. T. Cacioppo, M. E. Hughes, L. J. Waite, L. C. Hawkley, R. A. Thisted, Loneliness as a specific risk factor for depressive symptoms: Cross-sectional and longitudinal analyses. *Psychol. Aging* **21**, 140–151 (2006).
- K. C. F. Fone, M. V. Porkess, Behavioural and neurochemical effects of post-weaning social isolation in rodents—Relevance to developmental neuropsychiatric disorders. *Neurosci. Biobehav. Rev.* **32**, 1087–1102 (2008).
- G. A. Matthews, E. H. Nieh, C. M. Vander Weele, S. A. Halbert, R. V. Pradhan, A. S. Yosafat, G. F. Glober, E. M. Izadmeh, R. E. Thomas, G. D. Lacy, C. P. Wildes, K. M. Tye, Dorsal raphe dopamine neurons represent the experience of social isolation. *Cell* **164**, 617–631 (2016).
- L. Tomova, K. L. Wang, T. Thompson, G. A. Matthews, A. Takahashi, K. M. Tye, R. Saxe, Acute social isolation evokes midbrain craving responses similar to hunger. *Nat. Neurosci.* **23**, 1597–1605 (2020).
- L. Senst, D. Baimoukhametova, T.-L. Sterley, J. S. Bains, Sexually dimorphic neuronal responses to social isolation. *eLife* **5**, e18726 (2016).
- D. Vandervoort, Social isolation and gender. *Curr. Psychol.* **19**, 229–236 (2000).
- A. N. V. Ruigrok, G. Salimi-Khorshidi, M.-C. Lai, S. Baron-Cohen, M. V. Lombardo, R. J. Tait, J. Suckling, A meta-analysis of sex differences in human brain structure. *Neurosci. Biobehav. Rev.* **39**, 34–50 (2014).
- S. Bálint, P. Czobor, S. Komlósi, A. Mészáros, V. Simon, I. Bitter, Attention deficit hyperactivity disorder (ADHD): Gender-and age-related differences in neurocognition. *J. Psychol. Med.* **39**, 1337–1345 (2009).
- G. Wooten, L. Currie, V. Bovbjerg, J. Lee, J. Patrie, Are men at greater risk for Parkinson's disease than women? *J. Neurol. Neurosurg. Psychiatry* **75**, 637–639 (2004).
- J. M. Borland, L. M. Aiani, A. Norvelle, K. N. Grantham, K. O'Laughlin, J. I. Terranova, K. J. Frantz, H. Elliott Albers, Sex-dependent regulation of social reward by oxytocin receptors in the ventral tegmental area. *Neuropsychopharmacology* **44**, 785–792 (2019).
- A. Brancato, D. Bregman, H. F. Ahn, M. L. Pfau, C. Menard, C. Cannizzaro, S. J. Russo, G. E. Hodess, Sub-chronic variable stress induces sex-specific effects on glutamatergic synapses in the nucleus accumbens. *Neuroscience* **350**, 180–189 (2017).
- M. Asher, I. M. Aderka, Gender differences in social anxiety disorder. *J. Clin. Psychol.* **74**, 1730–1741 (2018).
- G. D. Greenberg, A. Laman-Maharg, K. L. Campi, H. Voigt, V. N. Orr, L. Schaal, B. C. Trainor, Sex differences in stress-induced social withdrawal: Role of brain derived neurotrophic factor in the bed nucleus of the stria terminalis. *Front. Behav. Neurosci.* **7**, 223–223 (2014).
- D. K. Oliver, K. Intson, D. Sargin, S. K. Power, J. M. Nabb, A. J. Ramsey, E. K. Lambe, Chronic social isolation exerts opposing sex-specific consequences on serotonin neuronal excitability and behaviour. *Neuropharmacology* **168**, 108015 (2020).
- T. R. Stratford, D. Wirtshafter, Ascending dopaminergic projections from the dorsal raphe nucleus in the rat. *Brain Res.* **511**, 173–176 (1990).
- M. E. Trulsson, M. S. Cannon, J. D. Raese, Identification of dopamine-containing cell bodies in the dorsal and median raphe nuclei of the rat brain using tyrosine hydroxylase immunocytochemistry. *Brain Res. Bull.* **15**, 229–234 (1985).
- K. W. Huang, N. E. Ochandarena, A. C. Philson, M. Hyun, J. E. Birnbaum, M. Cicconet, B. L. Sabatini, Molecular and anatomical organization of the dorsal raphe nucleus. *eLife* **8**, e46464 (2019).
- C. M. Vander Weele, C. A. Siciliano, G. A. Matthews, P. Namburi, E. M. Izadmeh, I. C. Espinel, E. H. Nieh, E. H. S. Schut, N. Padilla-Coreano, A. Burgos-Robles, C.-J. Chang, E. Y. Kimchi, A. Beyeler, R. Wichmann, C. P. Wildes, K. M. Tye, Dopamine enhances signal-to-noise ratio in cortical-brainstem encoding of aversive stimuli. *Nature* **563**, 397–401 (2018).
- I. B. Witten, E. E. Steinberg, S. Y. Lee, T. J. Davidson, K. A. Zalocusky, M. Brodsky, O. Yizhar, S. L. Cho, S. Gong, C. Ramakrishnan, G. D. Stuber, K. M. Tye, P. H. Janak, K. Deisseroth, Recombinase-driver rat lines: Tools, techniques, and optogenetic application to dopamine-mediated reinforcement. *Neuron* **72**, 721–733 (2011).
- H.-C. Tsai, F. Zhang, A. Adamantidis, G. D. Stuber, A. Bonci, L. de Lecea, K. Deisseroth, Phasic firing in dopaminergic neurons is sufficient for behavioral conditioning. *Science* **324**, 1080–1084 (2009).
- S. Bariselli, H. Hörnberg, C. Prévost-Solié, S. Musardo, L. Hatstatt-Burklé, P. Scheiffele, C. Bellone, Role of VTA dopamine neurons and neuregulin 3 in sociability traits related to nonfamiliar conspecific interaction. *Nat. Commun.* **9**, 3173 (2018).
- L. A. Gunaydin, L. Grosenick, J. C. Finkelstein, I. V. Kauvar, L. E. Fenno, A. Adhikari, S. Lammel, J. J. Mirzabekov, R. D. Airan, K. A. Zalocusky, K. M. Tye, P. Anikeeva, R. C. Malenka, K. Deisseroth, Natural neural projection dynamics underlying social behavior. *Cell* **157**, 1535–1551 (2014).
- R. Lin, J. Liang, R. Wang, T. Yan, Y. Zhou, Y. Liu, Q. Feng, F. Sun, Y. Li, A. Li, H. Gong, M. Luo, The raphe dopamine system controls the expression of incentive memory. *Neuron* **106**, 498–514.e8 (2020).
- J. R. Cho, J. B. Treweek, J. E. Robinson, C. Xiao, L. R. Bremner, A. Greenbaum, V. Gradinaru, Dorsal raphe dopamine neurons modulate arousal and promote wakefulness by salient stimuli. *Neuron* **94**, 1205–1219.e8 (2017).
- F. Groessl, T. Munsch, S. Meis, J. Griessner, J. Kaczanowska, P. Pliota, D. Kargl, S. Badurek, K. Kraitsy, A. Rassoulpour, J. Zuber, V. Lessmann, W. Haubensak, Dorsal tegmental dopamine neurons gate associative learning of fear. *Nat. Neurosci.* **21**, 952–962 (2018).
- S. Salgado, M. G. Kaplitt, The nucleus accumbens: A comprehensive review. *Stereotact. Funct. Neurosurg.* **93**, 75–93 (2015).
- C. R. Gerfen, D. J. Surmeier, Modulation of striatal projection systems by dopamine. *Annu. Rev. Neurosci.* **34**, 441–466 (2011).
- R. J. Smith, M. K. Lobo, S. Spencer, P. W. Kalivas, Cocaine-induced adaptations in D1 and D2 accumbens projection neurons (a dichotomy not necessarily synonymous with direct and indirect pathways). *Curr. Opin. Neurobiol.* **23**, 546–552 (2013).
- G. Dolen, A. Darvishzadeh, K. W. Huang, R. C. Malenka, Social reward requires coordinated activity of nucleus accumbens oxytocin and serotonin. *Nature* **501**, 179–184 (2013).
- D. L. Wallace, M.-H. Han, D. L. Graham, T. A. Green, V. Vialou, S. D. Iñiguez, J.-L. Cao, A. Kirk, S. Chakravarty, A. Kumar, V. Krishnan, R. L. Neve, D. C. Cooper, C. A. Bolaños, M. Barrot, C. A. McClung, E. J. Nestler, CREB regulation of nucleus accumbens excitability mediates social isolation-induced behavioral deficits. *Nat. Neurosci.* **12**, 200–209 (2009).
- S. A. Josselyn, S. Tonegawa, Memory engrams: Recalling the past and imagining the future. *Science* **367**, eaaw4325 (2020).
- J.-H. Choi, S.-E. Sim, J.-I. Kim, D. I. Choi, J. Oh, S. Ye, J. Lee, T. H. Kim, H.-G. Ko, C.-S. Lim, B.-K. Kaang, Interregional synaptic maps among engram cells underlie memory formation. *Science* **360**, 430–435 (2018).
- T. J. Ryan, D. S. Roy, M. Pignatelli, A. Arons, S. Tonegawa, Engram cells retain memory under retrograde amnesia. *Science* **348**, 1007–1013 (2015).
- X. Liu, S. Ramirez, P. T. Pang, C. B. Puryear, A. Govindarajan, K. Deisseroth, S. Tonegawa, Optogenetic stimulation of a hippocampal engram activates fear memory recall. *Nature* **484**, 381–385 (2012).
- E. Koya, S. A. Golden, B. K. Harvey, D. H. Guez-Barber, A. Berkow, D. E. Simmons, J. M. Bossert, S. G. Nair, J. L. Uejima, M. T. Marin, T. B. Mitchell, D. Farquhar, S. C. Ghosh, B. J. Mattson, B. T. Hope, Targeted disruption of cocaine-activated nucleus accumbens neurons prevents context-specific sensitization. *Nat. Neurosci.* **12**, 1069–1073 (2009).

39. F. C. Cruz, K. R. Babin, R. M. Leao, E. M. Goldart, J. M. Bossert, Y. Shaham, B. T. Hope, Role of nucleus accumbens shell neuronal ensembles in context-induced reinstatement of cocaine-seeking. *J. Neurosci.* **34**, 7437–7446 (2014).
40. N. R. Wall, P. A. Neumann, K. T. Beier, A. K. Mokhtari, L. Luo, R. C. Malenka, Complementary genetic targeting and monosynaptic input mapping reveal recruitment and refinement of distributed corticostriatal ensembles by cocaine. *Neuron* **104**, 916–930.e5 (2019).
41. G. E. Gillies, S. McArthur, Estrogen actions in the brain and the basis for differential action in men and women: A case for sex-specific medicines. *Pharmacol. Rev.* **62**, 155–198 (2010).
42. A. Riecher-Rössler, H. Häfner, M. Stumbaum, K. Maurer, R. Schmidt, Can estradiol modulate schizophrenic symptomatology? *Schizophr. Bull.* **20**, 203–214 (1994).
43. B. Hille, Ionic channels in excitable membranes. Current problems and biophysical approaches. *Biophys. J.* **22**, 283–294 (1978).
44. D. A. A. MacLaren, R. W. Browne, J. K. Shaw, S. K. Radhakrishnan, P. Khare, R. A. España, S. D. Clark, Clozapine N-oxide administration produces behavioral effects in long-Evans rats: Implications for designing DREADD experiments. *eNeuro* **3**, ENEURO.0219-16.2016 (2016).
45. S. Park, E. E. Kramer, V. Mercaldo, A. J. Rashid, N. Insel, P. W. Frankland, S. A. Josselyn, Neuronal allocation to a hippocampal engram. *Neuropsychopharmacology* **41**, 2987–2993 (2016).
46. G. van Haasteren, S. Li, S. Ryser, W. Schlegel, Essential contribution of intron sequences to Ca<sup>2+</sup>-dependent activation of *c-fos* transcription in pituitary cells. *Neuroendocrinology* **72**, 368–378 (2000).
47. R. Loew, N. Heinz, M. Hampf, H. Bujard, M. Gossen, Improved Tet-responsive promoters with minimized background expression. *BMC Biotechnol.* **10**, 81 (2010).
48. L. G. Reijmers, B. L. Perkins, N. Matsuo, M. Mayford, Localization of a stable neural correlate of associative memory. *Science* **317**, 1230–1233 (2007).
49. X. Zhou, M. Vink, B. Klaver, B. Berkhout, A. T. Das, Optimization of the Tet-On system for regulated gene expression through viral evolution. *Gene Ther.* **13**, 1382–1390 (2006).
50. K. Yoshimoto, W. J. McBride, Regulation of nucleus accumbens dopamine release by the dorsal raphe nucleus in the rat. *Neurochem. Res.* **17**, 401–407 (1992).
51. P. De Deurwaerdere, L. Stinus, U. Spampinato, Opposite change of in vivo dopamine release in the rat nucleus accumbens and striatum that follows electrical stimulation of dorsal raphe nucleus: Role of 5-HT<sub>3</sub> receptors. *J. Neurosci.* **18**, 6528–6538 (1998).
52. Y. Zhou, H. Zhu, Z. Liu, X. Chen, X. Su, C. Ma, Z. Tian, B. Huang, E. Yan, X. Liu, L. Ma, A ventral CA1 to nucleus accumbens core engram circuit mediates conditioned place preference for cocaine. *Nat. Neurosci.* **22**, 1986–1999 (2019).
53. D. I. Choi, J. Kim, H. Lee, J.-i. Kim, Y. Sung, J. E. Choi, S. J. Venkat, P. Park, H. Jung, B.-K. Kaang, Synaptic correlates of associative fear memory in the lateral amygdala. *Neuron* **109**, 2717–2726.e3 (2021).
54. H. Jung, S.-W. Kim, M. Kim, J. Hong, D. Yu, J. H. Kim, Y. Lee, S. Kim, D. Woo, H.-S. Shin, B. O. Park, W. D. Heo, Noninvasive optical activation of Flp recombinase for genetic manipulation in deep mouse brain regions. *Nat. Commun.* **10**, 314 (2019).
55. J. Lucchetti, C. Fracasso, C. Balducci, A. Passoni, G. Forloni, M. Salmona, M. Gobbi, Plasma and brain concentrations of doxycycline after single and repeated doses in wild-type and APP23 mice. *J. Pharmacol. Exp. Ther.* **368**, 32–40 (2019).
56. M. Pignatelli, A. Bonci, Role of dopamine neurons in reward and aversion: A synaptic plasticity perspective. *Neuron* **86**, 1145–1157 (2015).
57. C. Soares-Cunha, B. Coimbra, A. David-Pereira, S. Borges, L. Pinto, P. Costa, N. Sousa, A. J. Rodrigues, Activation of D2 dopamine receptor-expressing neurons in the nucleus accumbens increases motivation. *Nat. Commun.* **7**, 11829 (2016).
58. G. D. Stuber, T. S. Hnasko, J. P. Britt, R. H. Edwards, A. Bonci, Dopaminergic terminals in the nucleus accumbens but not the dorsal striatum corelease glutamate. *J. Neurosci.* **30**, 8229–8233 (2010).
59. F. Tecuapetla, J. C. Patel, H. Xenias, D. English, I. Tadros, F. Shah, J. Berlin, K. Deisseroth, M. E. Rice, J. M. Tepper, T. Koos, Glutamatergic signaling by mesolimbic dopamine neurons in the nucleus accumbens. *J. Neurosci.* **30**, 7105–7110 (2010).
60. A. G. Dougalis, G. A. C. Matthews, M. W. Bishop, F. Brischoux, K. Kobayashi, M. A. Ungless, Functional properties of dopamine neurons and co-expression of vasoactive intestinal polypeptide in the dorsal raphe nucleus and ventro-lateral periaqueductal grey. *Eur. J. Neurosci.* **36**, 3322–3332 (2012).
61. J. I. Broussard, Co-transmission of dopamine and glutamate. *J. Gen. Physiol.* **139**, 93–96 (2012).
62. N. X. Tritsch, B. L. Sabatini, Dopaminergic modulation of synaptic transmission in cortex and striatum. *Neuron* **76**, 33–50 (2012).
63. P. Voorn, C. R. Gerfen, H. J. Groenewegen, Compartmental organization of the ventral striatum of the rat: Immunohistochemical distribution of enkephalin, substance P, dopamine, and calcium-binding protein. *J. Comp. Neurol.* **289**, 189–201 (1989).
64. L. Heimer, G. F. Alheid, J. S. de Olmos, H. J. Groenewegen, S. N. Haber, R. E. Harlan, D. S. Zahm, The accumbens: Beyond the core-shell dichotomy. *J. Neuropsychiatry Clin. Neurosci.* **9**, 354–381 (1997).
65. S. R. Sesack, A. A. Grace, Cortico-Basal Ganglia reward network: Microcircuitry. *Neuropsychopharmacology* **35**, 27–47 (2010).
66. G. Heymann, Y. S. Jo, K. L. Reichard, N. McFarland, C. Chavkin, R. D. Palmiter, M. E. Soden, L. S. Zweifel, Synergy of distinct dopamine projection populations in behavioral reinforcement. *Neuron* **105**, 909–920.e5 (2020).
67. T. C. Francis, H. Yano, T. G. Demarest, H. Shen, A. Bonci, High-frequency activation of nucleus accumbens D1-MSNs drives excitatory potentiation on D2-MSNs. *Neuron* **103**, 432–444.e3 (2019).
68. T. Okuyama, T. Kitamura, D. S. Roy, S. Itoharu, S. Toneyawa, Ventral CA1 neurons store social memory. *Science* **353**, 1536–1541 (2016).
69. I. D. Neumann, R. Landgraf, Balance of brain oxytocin and vasopressin: Implications for anxiety, depression, and social behaviors. *Trends Neurosci.* **35**, 649–659 (2012).
70. C. Kasari, L. Sterling, Loneliness and social isolation in children with autism spectrum disorders, and *The Handbook of Solitude: Psychological Perspectives on Social Isolation, Social Withdrawal, and Being Alone*, R. J. Coplan, J. C. Bowker, Eds. (Wiley Blackwell, 2014), pp. 409–426.
71. G. I. Orsmond, P. T. Shattuck, B. P. Cooper, P. R. Sterzing, K. A. Anderson, Social participation among young adults with an autism spectrum disorder. *J. Autism Dev. Disord.* **43**, 2710–2719 (2013).
72. M. Mitjans, M. Begemann, A. Ju, E. Dere, L. Wüstefeld, S. Hofer, I. Hassouna, J. Balkenhol, B. Oliveira, S. van der Auwera, R. Tammer, K. Hammerschmidt, H. Völzke, G. Homuth, F. Ceconi, K. Chowdhury, H. Grabe, J. Frahm, S. Boretius, T. Dandekar, H. Ehrenreich, Sexual dimorphism of AMBRA1-related autistic features in human and mouse. *Transl. Psychiatry* **7**, e1247 (2017).
73. D. M. Werling, N. N. Parikshak, D. H. Geschwind, Gene expression in human brain implicates sexually dimorphic pathways in autism spectrum disorders. *Nat. Commun.* **7**, 10717 (2016).
74. J. Lindeberg, D. Usoskin, H. Bengtsson, A. Gustafsson, A. Kylberg, S. Söderström, T. Ebendal, Transgenic expression of Cre recombinase from the tyrosine hydroxylase locus. *Genesis* **40**, 67–73 (2004).
75. J. H. Lee, E. A. Ribeiro, J. Kim, B. Ko, H. Kronman, Y. H. Jeong, J. K. Kim, P. H. Janak, E. J. Nestler, J. W. Koo, J. H. Kim, Dopaminergic regulation of nucleus accumbens cholinergic interneurons demarcates susceptibility to cocaine addiction. *Biol. Psychiatry* **88**, 746–757 (2020).
76. S. Gong, C. Zheng, M. L. Doughty, K. Losos, N. Didkovsky, U. B. Schambra, N. J. Nowak, A. Joyner, G. Leblanc, M. E. Hatten, N. Heintz, A gene expression atlas of the central nervous system based on bacterial artificial chromosomes. *Nature* **425**, 917–925 (2003).
77. M. T. Hasan, F. Althammer, M. S. da Gouveia, S. Goyon, M. Eliava, A. Lefevre, D. Kerspern, J. Schimmer, A. Raftogianni, J. Wahis, H. S. Knobloch-Bollmann, Y. Tang, X. Liu, A. Jain, V. Chavant, Y. Goumon, J.-M. Weislogel, R. Hurlmann, S. C. Herpertz, C. Pitzer, P. Darbon, G. K. Dogbevia, I. Bertocchi, M. E. Larkum, R. Sprengel, H. Bading, A. Charlet, V. Grinevich, A fear memory engram and its plasticity in the hypothalamic oxytocin system. *Neuron* **103**, 133–146.e8 (2019).
78. C.-S. Lim, M. J. Kim, J. E. Choi, M. A. Islam, Y.-K. Lee, Y. Xiong, K.-W. Shim, J.-E. Yang, R. U. Lee, J. Lee, P. Park, J.-H. Kwak, H. Seo, C. H. Kim, J.-H. Lee, Y.-S. Lee, S.-K. Hwang, K. Lee, J.-A. Lee, B.-K. Kaang, Dysfunction of NMDA receptors in neuronal models of an autism spectrum disorder patient with a DSCAM mutation and in Dscam-knockout mice. *Mol. Psychiatry* **26**, 7538–7549 (2021).
79. J. Park, C.-S. Lim, H. Seo, C.-A. Park, M. Zhuo, B.-K. Kaang, K. Lee, Pain perception in acute model mice of Parkinson's disease induced by 1-methyl-4-phenyl-1,2,3,6-tetrahydropyridine (MPTP). *Mol. Pain* **11**, 28 (2015).
80. M. T. Ke, Y. Nakai, S. Fujimoto, R. Takayama, S. Yoshida, T. S. Kitajima, M. Sato, T. Imai, Super-resolution mapping of neuronal circuitry with an index-optimized clearing agent. *Cell Rep.* **14**, 2718–2732 (2016).
81. F. Sun, J. Zhou, B. Dai, T. Qian, J. Zeng, X. Li, Y. Zhuo, Y. Zhang, Y. Wang, C. Qian, K. Tan, J. Feng, H. Dong, D. Lin, G. Cui, Y. Li, Next-generation GRAB sensors for monitoring dopaminergic activity in vivo. *Nat. Methods* **17**, 1156–1166 (2020).

**Acknowledgments:** We thank K. Tye and G. Matthews for critical comments and suggestions on an earlier version of the manuscript. **Funding:** This work was supported by the National Honor Scientist Program (NRF-2012R1A3A1050385) of Korea. **Author contributions:** J.E.C., D.I.C., and B.-K.K. contributed to the study design and wrote the paper. J.E.C. designed and conducted all the animal behavior and electrophysiology experiments. D.I.C. conducted fiber photometry, subcloning, virus preparation, image analysis, and stereotaxic surgery. J.L., Jooyoung Kim, M.J.K., I.H., H.J., Y.S., Ji-il Kim, T.K., N.-K.Y., and S.-H.L. assisted with virus preparation, stereotaxic surgery, immunohistochemistry, and data analysis. H.K.C., J.W.K., and J.-H.K. contributed to the interpretation of the data and revising the manuscript. **Competing interests:** The authors declare that they have no competing interests. **Data and materials availability:** All data needed to evaluate the conclusions in the paper are present in the paper and/or the Supplementary Materials.

Submitted 11 March 2022  
Accepted 25 August 2022  
Published 12 October 2022  
10.1126/sciadv.abo7527